Abstract

Title of thesis: Dynamics of Elastic Capsules in Cross-Junction and T-Junction Microfluidic Channels

Pompon Mputu Udipabu, Master of Science, 2017

Thesis directed by: Professor Panagiotis Dimitrakopoulos
Department of Chemical and Biomolecular Engineering

In this dissertation, we investigate via numerical computations the dynamics of elastic capsules (made from a thin strain-hardening elastic membrane) in two microfluidic channels of cross-junction and T-junction geometries. For the cross-junction microfluidic channel, we consider an initially spherical capsule with a size smaller than the cross-section of the square channels comprising the cross-junction, and investigate the effects of the capsule size, flow rate, and lateral flow rates on the transient dynamics and deformation of low-viscosity and equiviscous capsules. In addition, we also study the effects of viscosity ratio on the transient capsule dynamics and deformation. Our investigation shows that the intersecting lateral flows at the cross-junction act like a constriction. Larger capsules, higher flow rates and higher intersecting lateral flows result in stronger hydrodynamic forces that cause a significant capsule deformation, i.e., the capsule's length increases while its height decreases significantly. The capsule obtains different dynamic shape transitions due to the asymmetric shape of the cross-junction. Larger capsules take more time to pass through the cross-junction owning to the higher flow blocking. As the viscosity ratio decreases, the capsule's transient deformation increases and a tail formation develops transiently, especially for low-viscosity capsules owing to the normal-stress effects of the surrounding fluid on the capsule's interface. However, the viscosity ratio does not affect much the capsule velocity due to a weak inner circulation. Our findings suggest that the tail formation of low-viscosity capsule may promote

membrane breaking and thus drug release of pharmaceutical capsules in the micro-circulation.

Furthermore, we investigate via numerical computations the motion of an elastic capsule (made from an elastic membrane obeying the strain-hardening Skalak law) flowing inside a microfluidic T-junction device. In particular, we consider the effects of the capsule size, flow rate, lateral flow rate, and fluid viscosity ratio on the motion of the capsule in the T-junction micro-channel. As the capsule's initial lateral position increases, the capsule moves faster and reaches different final lateral positions. As the capsule size increases, the gap between the capsule's surface and the channel wall decreases. This results in the development of stronger hydrodynamic forces and a decrease in the capsule velocity due to flow blocking. As the capsule size increases, there is a small lateral migration towards the micro-channel centerline, which is the low-shear region of the T-junction micro-channel. This migration is in agreement with experimental and numerical studies on non-inertial lateral migration of vesicles in bounded Poiseuille flow by Coupier *et al.* [13] who showed that the combined effects of the walls and of the curvature of the velocity profile induce a lateral migration toward the centerline of the channel. As the capillary number Ca increases, the stronger hydrodynamic forces cause the capsule to extend along the flow direction (i.e., the capsule's length L_x increases as the capsule enters the T-junctions and decreases as the capsule exits the T-junction). There is a small lateral migration away from the micro-channel centerline as the flow rate Ca increases. The capsule lateral position z_c, main-flow velocity U_x and migration velocity U_z are practically not affected by the fluids viscosity ratio λ. As the channel's lateral flow rate increases, the capsule migrates downwards towards the bottom of the device. Our findings on the lateral migration in the T-junction micro-channel suggest that there is a great potential for designing a T-junction microfluidic device that can be used to manipulate artificial and biological capsules.

Dynamics of Elastic Capsules in Cross-Junction and T-Junction Microfluidic Channels

by

Pompon Mputu Udipabu

Dissertation submitted to the Faculty of the Graduate School of the
University of Maryland, College Park in partial fulfillment
of the requirements for the degree of
Master of Science
2017

Advisory Committee:
Professor Panagiotis Dimitrakopoulos, Chair
Professor Srinivasa R. Raghavan
Professor Jeffery B. Klauda

© Copyright by
Pompon Mputu Udipabu
2017

Acknowledgments

It would not have been possible to finish my dissertation without the guidance of my advisor, encouragement from friends and support from my family.

First, I would like to express my deepest gratitude to my advisor, Professor Panagiotis Dimitrakopoulos for his excellent guidance, patience, caring and support throughout this journey. As someone who is a full-time Process Engineer at Merck, I am sure it would not have been possible without his help and patience.

Besides my advisor, I would also like to thank the members of our research lab, Abdollah Koolivand and Yiyang Wang for their encouragement, insightful comments and friendly suggestions.

Last but not the least, I would like to thank my parents and family for their love and support during my graduate studies.

The numerical computations were performed on multiprocessor computers provided by the Extreme Science and Engineering Discovery Environment (XSEDE) which is supported by the National Science Foundation. The author also acknowledges the University of Maryland supercomputing resources (http://www.it.umd.edu/hpcc) made available for conducting the research reported in this dissertation.

Contents

List of Figures

List of Abbreviations

α_p	Prestress parameter
$\Delta\boldsymbol{f}$	Surface stress vector
Δt	Time step
λ	Viscosity ratio
λ_α	Stretch ratio
μ	Ambient viscosity
σ	Stress tensor
τ_α^P	Principal tensions ($\alpha = 1, 2$)
τ	In-plane stress resultant
a	Capsule radius
C	Dimensionless area-dilatation modulus
Ca	Elastic capillary number
G_s	Shear modulus
G_a	Area-dilatation modulus
h	Gap between the solid particle's surface and the solid wall
ℓ_x	Half-length of the channel
ℓ_y	Half-width of the channel
ℓ_z	Half-height of the channel
L_x	Capsule length
L_y	Capsule width
L_z	Capsule height
$\boldsymbol{n}$	Surface unit normal vector
N_B	Number of basis points for spectral interpolation
N_E	Number of spectral elements
ΔP	Pressure difference
ΔP^0	Pressure difference in the absence of the soft particle
ΔP^+	Additional pressure difference, $\Delta P^+ = \Delta P - \Delta P^0$
ρ	Density
$\boldsymbol{S}$	Stokeslet solution for the velocity
$\boldsymbol{T}$	Stokeslet solution for the stress
$\boldsymbol{u}$	Velocity
$\boldsymbol{u}^\infty$	Undisturbed velocity
$\mathcal{U}$	Average undisturbed velocity in a microchannel

Chapter 1: Introduction

A capsule consists of an internal liquid droplet enclosed by a thin elastic membrane [48]. Under external fluid flow, capsules can be deformed and obtain many features observed for biological cells (i.e., bio-concave disc shape of red blood cells). As a result, they are usually used as a simplified model to study and understand the nature of the hemodynamic forces exerted on vascular endothelial cells or leukocytes adhering to the surface of blood vessels and the dynamics of erythrocytes in shear flows [23, 24, 56], to model and simulate red blood cell motion in micro-vessels and bifurcations, and to study the motion of platelets in the bloodstream [47]. Biological capsules such as red blood cells (RBC) are usually enclosed by a thin solid membrane with complicated structure. For instance, the red blood cell membrane consists of a phospholipid bilayer containing internal membrane proteins and an underlying membrane skeleton [42]. It is of interest to note that one of the RBC membrane properties, the high deformability of the membrane, is known to play a key role in the oxygen and carbon dioxide exchange between the micro-circulation and the body tissues. It allows the RBC to undergo extensive deformation without rupture in the constricted vascular capillary vessels, enabling it to effectively perform its function of oxygen and other respiratory gases delivery to and from the tissues.

In recent years considerable studies have been dedicated to understand the interfacial dynamics of capsules suspended in confined geometries [3, 48]. This is attributed to the need in utilizing capsules in the pharmaceutical, cosmetic, and food industries for encapsulation and controlled release of active ingredients, flavors or aromas [1, 14, 15, 37, 41, 57]. Encapsulation consists of enclosing some internal contents with a semipermeable membrane. The internal contents are thus protected from the external environment and can be released at a specific and desirable time. The controlled release can occur by breaking up suddenly the capsule membrane by the fluid flow or by diffusing continuously internal contents through the membrane [3].

Understanding the interfacial dynamics of capsules also presents numerous biomedical interests. Although these biomedical interests are motivated by in vivo biomedical experiments such as understanding the dynamics of erythrocytes in shear flows [23, 24, 56], simulating red blood cell motion in microvessels and bifurcations [47], in vitro understanding has received increasing attention in the lab-on-chip technologies [45]. Microfluidic approaches have led to many developments toward lab-on-chip technologies. The basic objective of these approaches is to miniaturize laboratory experiments and reduce the cost, processing times, and volume of fluid used in those experiments [19]. These approaches such as fabrication of micro-capsules with desirable properties [40, 50], encapsulation of cell culture for artificial organs growth [51], separation and sorting of cells [38], are seen as promising tools in diagnostics, high-throughput screening, drug delivery systems and drug discovery [44, 45, 48].

Since capsules are widely used as a mimicking model to study biological cells and are of great importance for pharmaceutical, cosmetic and food industries, many studies have been conducted on different fabrication techniques of artificial capsule [44]. Capsules of different physical properties (e.g. shape, size and stability) can be artificially produced in the laboratory depending on fabrication parameters, membrane materials and encapsulation techniques.

Artificial capsules can be fabricated through interfacial polymerization of a liquid droplet. First, a liquid droplet of required size or shape is fabricated. Then the liquid droplet is cross-linked with another liquid at either T-junction or cross-junction microchannels. Capsules obtained through this process are often enclosed by a thin polymerized membrane with physical properties that depends on the employed synthesis strategies [3]. Few properties can be determined experimentally. The size of artificial capsules varies from a few micrometers to a few millimeters, and the rheological properties of the internal content can be measured independently (e.g. , by breaking the capsules). However, elastic membrane properties are quite difficult to measure owing to capsule size and fragility [48]. Some powerful models are thus needed to assess elastic membrane properties of artificial capsules. Based on computational investigation, Dimitrakopoulos *et al.*proposed a new methodology to determine a membrane's shear modulus, independent of its area-dilatation modulus, by flowing strain-hardening capsules in a converging micro-capillary of comparable size under Stokes flow conditions [20]. Other powerful models are also needed to design and optimize artificial capsules for transporting and releasing internal contents of capsules as demanded in pharmaceutical, cosmetic and food industries. As a result, the computational study of the interfacial dynamics of elastic capsules represents a fundamental problem. This requires a comprehension of the dynamics and deformation of elastic capsules in confined solid ducts such as microfluidic channels.

The dynamics and deformation of capsule in solid ducts are determined by the nonlinear coupling of the deforming hydrodynamic forces with the restoring interfacial forces of the particle membrane [28]. Note that this coupling is mutual. On one hand, the hydrodynamic forces deform the capsule and on the other hand, the deformed capsule changes the boundary conditions at the interface. As a result of this interplay of opposing forces, the capsule deforms and takes different dynamic transition shapes.

Experiments have been conducted on initially spherical artificial capsules flowing in cylindrical and square-section microfluidic channels. Risso *et al.*experimentally investigated the motion and deformation of an initially slightly over-inflated bioartificial capsule made of covalently linked human serum albumin (HSA) and alginate in a cylindrical microfluidic pore. They found that by increasing the capillary number Ca at a fixed capsule size, the capsule deforms and takes different dynamic transition shapes from bullet-like shape to parachute-like shape [49]. Lefebvre *et al.*experimentally investigated the effects of flow rate on deformation of microcapsules made of crossed-linked ovalbumin flowing inside cylindrical and square-section microchannels in order to determine the membrane mechanical properties of microcapsules. In all these studies, the capsule's velocity and deformed profile were obtained, and the membrane shear elastic modulus for a neo-Hookean constitutive law was determined independent from capsule size or deformation [7]. Hu *et al.*considered an initially spherical capsule with diameter smaller than that used by Lefebvre *et al.*and made of crossed-linked ovalbumin. They studied the effect of capillary number Ca on the motion and deformation of a capsule flowing in a square-section microchannel. Capsule profiles and the corresponding velocities were obtained, and the shear elastic modulus of the membrane was determined by comparison of experimental and numerical results [4].

Numerous bioengineering and industrial interests have also motivated efforts to computationally study the dynamics and motion of capsules and biological capsules in a confined fluid flow. The theoretical studies were initiated by Barthès-Biesel in 1980 [12]. Using a regular perturbation technique, she studied the effects of shear rate, viscosity ratio, and the membrane elastic coefficient on the deformation and orientation of microcapsule in a simple linear shear flow. An analytical asymptotic solution to the problem was obtained and results predicted the tank-treading motion of capsule. Her work revealed that the capsule orientation and deformation depend on capsule physical properties such as the viscosity ratio and elastic properties. The more viscous capsule was shown to be more titled toward the streamlines. Using the lubrication approximation, Secomb *et al.*studied the steady axisymmetric deformation of red blood cells flowing in a narrow cylindrical channel [55]. The lubrication theory was used to describe the flow of the suspending fluid in the gap between the cells and the channel wall. They studied the effect of flow rate on the cell shape and apparent viscosity. Their results showed that the cell shape and apparent viscosity were independent of flow rate at moderate and high cell velocities. However, at lower flow velocities, membrane shear and bending resistances become increasingly important, and apparent viscosity was shown to increase with decreasing flow rate.

Furthermore, several two dimensional (2D) models were developed to study the biological capsule motion and deformation under various confined flows. Using a finite element numerical method in 2D, Sugihara-Seki et al. [54] studied the effect of tank-treading motion on an idealized zipper-type flow. They found a critical viscosity ratio that impacted the membrane tank-treading motion of red blood cells. If the viscosity ratio was lower than than the critical value, the zipper-type arrangements of red blood cells in capillaries were stabilized by the membrane tank-treading motion. When the tank-treading motion was inhibited by increasing the viscosity ratio above the critical value, a cyclic oscillatory motion of red cells was observed. The critical viscosity ratio was shown to increase if the channel was narrowed or if the spacing between cells was reduced. Using the immersed boundary method, Bagchi [2] studied the motion of an individual red blood cell in suspension and the collective motion of many cells in small vessels. His numerical results correctly was in agreement with the Fahraeus-Lindqvist effect. The tank-treading and tumbling motion, and the lateral migration of red blood cells were observed. However, Bagchi's 2D model had several limitations. For instance, it was questionable on how the simplified 2D model could provide accurate results of motion and deformation of red blood cells which are inherently three-dimensional(3D). A full 3D model is necessary to describe the dynamics and deformation of capsule in confined flows.

Over the years, great progress has been made to study the dynamics and deformation of capsule in 3D. Spherical capsules made of elastic membranes obeying either an Neo-Hookean (NH) or Skalak (SK) law, and flowing in a cylindrical pore have been studied. Barthès-Biesel *et al.*studied the effects of capsule shape and size, membrane rheology, membrane elasticity, and viscosity ratio of bioartificial capsule flowing into a cylindrical pore, and neglected the internal osmotic pressure and bending resistance of the membrane [11]. They found that the entrance of the capsule in the pore is very sensitive to the capsule shape and volume. The viscosity ratio is important where blocking of the pore is apparently reached. The effect of capsule rheology is significant when the deformations are very large. Lefevre *et al.*further considered the effect of osmotic pressure on the motion of bioartificial capsule flowing into a cylindrical pore. They found that the presence of an osmotic pressure and membrane pre-stress significantly alters the dynamics of capsules through small pores [9]. In addition, the motion and deformation of capsules in a square-section microchannel have been studied for NH and SK membrane laws. Hu *et al.* [5] studied the motion and deformation of a spherical elastic capsule flowing in a microfluidic square-section pore and compared the results to the circular cross-section. The capsule membrane was described by the NH constitutive law with negligible membrane bending resistance and their results were shown to qualitatively agree with those observed for the flow of capsules in cylindrical tubes [11]. However, for the same size ratio and flow rate, a capsule was more deformed in a circular than in a square cross-section pore. Using a boundary integral method, the elastic capsule flow in a square-section channel was investigated by Kuriakose and Dimitrakopoulos [28]. An initial spherical capsule obeying the Skalak strain-hardening membrane law with negligible membrane bending resistance was slightly inflated and pre-stressed by a positive osmotic pressure difference between the internal and external fluids. They examined the effects of capsule size and capillary number on the capsule steady states in a square-section channel and compared results with those observed in a cylindrical channel. They also found that the capsule motion in a square channel is similar to and thus governed by the same scaling laws of the capsule motion in a cylindrical channel. Overall, it is important to note that in all of those studies (i.e., the flow of a capsule in an either cylindrical or square channel), the main result is that an initially spherical capsule takes a parachute-like or bullet-like shape in a square or cylindrical channel and adapts to the boundary confinement and the hydrodynamic forces. It is easier to deform a capsule with an neo-Hooken than with an Skalak membrane law and the osmotic prestress significantly decreases the deformability of a capsule.

In addition, the motion and deformation of capsules in a microfluidic rectangular-section and constriction channels have been studied in our group. Kuriakose and Dimitrakopoulos investigated computationally the deformation of an elastic capsule in a rectangular microfluidic channel. They found that the deformation of capsule in a rectangular channel is different from that in a square or cylindrical channel. For example, in a rectangular channel, the capsule extended mainly along the less-confined lateral direction of the channel cross-section. This is in contrast to the bullet or parachute shape developed in a square or cylindrical channel where the capsule extends along the flow direction while in a rectangular channel, a pebble-like shape was observed [26]. Furthermore, Park and Dimitrakopoulos also investigated the transient dynamics of an elastic capsule flowing in a square microchannel with a rectangular constriction. They showed that the confinement and expansion dynamics of the fluid flow in the constriction region results in a rich deformation behavior for the capsule, from an elongated shape at the constriction entrance, to a flattened parachute shape at its exit.

In this dissertation, we investigate computationally the transient dynamics of an elastic capsule flowing along the centerline of a cross-junction microchannel and also investigate the motion of an elastic capsule in a T-junction microchannel. Our motivation is to develop powerful model that is needed for design and optimization of the fabrication of artificial capsules that are used for transporting and releasing the internal contents as demanded in pharmaceutical, cosmetic and food industries. The control release of internal capsule content is of course essential for the design of artificial capsules through interfacial polymerization. Our investigation of the transient dynamics of an elastic capsule in a cross-junction channel shows that the intersecting lateral flows at the cross-junction act like a constriction. Thus, the stronger hydrodynamic forces owning to the intersecting lateral flows cause a significant capsule deformation. The capsule obtains different transitional shapes due to the asymmetric shape of the cross-junction. As the viscosity ratio decreases, the capsule's transient deformation increases and a tail formation develops transiently, especially for the low-viscosity capsule. This tail formation increases as the capsule size increases or lateral flow rates increases. Our findings suggest that the tail formation of low-viscosity capsule may promote membrane breaking and thus drug release of pharmaceutical capsules in the microcirculation. Second, the T-junction can be used during the cross-linking process to fabricate artificial capsules of desirable properties and capsules are then separated based on the capsule size. Our investigation shows that the capsule moves faster and reaches different final lateral position as the capsule initial lateral position increases. As the capsule size increases, the gap between the capsule surface and channel walls decreases. This results in development of stronger hydrodynamic forces and a decrease in the capsule velocity. As the channel lateral flow rate increases, the capsule migrates more towards the bottom of the exit channel. A small lateral migration towards the centerline is observed as the capsule size increases. Our investigation suggests that this lateral migration can be used to sort out artificial and biological capsules based on the size in the T-junction microchannel.

In summary, the present work is outlined as follows: In chapter 2, we discuss the mathematical framework of the problem. Topics include the governing equations, boundary-integral formulation, and membrane dynamics which we employ in our numerical method. We also discuss the three-dimensional Membrane Spectral Boundary Element (MSBE) method. Chapter 3 employs the MSBE method to study computationally the transient dynamics of an elastic capsule flowing along the centerline of a cross-junction microchannel. In particular, we consider an initially spherical capsule with a size smaller than the cross-section of the square channels comprising the cross-junction, and investigate the effects of the capsule size, flow rate, lateral flow rate, and fluid viscosity ratio on the transient capsule dynamics and deformation. We analyze our results by looking at capsule shape transitions, capsule geometrical properties (i.e., capsule's dimensions and profile curvatures) and capsule velocity U_x as the capsule enters and exits the cross-junction channel. Chapter 4 investigates the effects of the capsule initial lateral position, the capsule size, the flow rate, the lateral flow rate, and the fluid viscosity ratio on the motion of elastic capsule in the T-junction microchannel. We present our results by considering capsule geometrical properties (i.e., capsule's dimensions), the lateral position, the capsule velocity U_x, and the capsule lateral migration velocity U_z.

Chapter 2: Mathematical formulation

2.1 Stokes Flow and Boundary Intergral Formulation

We consider a three-dimensional capsule suspended in a simple shear flow, thus subjected to hydrodynamic stresses as shown in Figure 2.1. The capsule's interior and exterior fluids are incompressible Newtonian fluids, with viscosites $\lambda\mu$ and μ, and have equal density ρ (i.e., no buoyancy and sedimentation effects). We define the capsule size by $a = (3V/4\pi)^{1/3}$ where V is the capsule volume. It is important to assume that the capsule has a negligible membrane permeability (i.e., no flow through the capsule membrane) and its volume is constant.

At low-Reynolds number, the inertial terms in the Navier-Stokes equations are neglected and the governing equations are the Stokes equations and continuity given

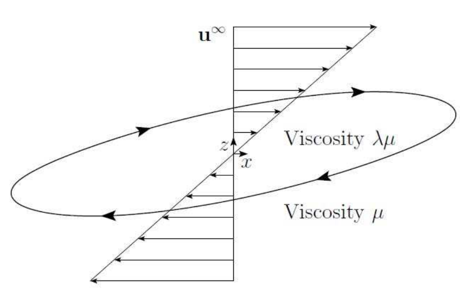

Figure 2.1: Illustration of an elastic capsule with internal viscosity $\lambda\mu$ suspended in an infinite fluid with viscosity μ in simple shear flow and subjected to hydrodynamic stresses. $\boldsymbol{u}^\infty$ is the undisturbed fluid velocity field.

by,

$$\nabla \cdot \boldsymbol{\sigma} = -\nabla p + \mu \nabla^2 \boldsymbol{u} = 0 \tag{2.1}$$

$$\nabla \cdot \boldsymbol{u} = 0 \tag{2.2}$$

where $\boldsymbol{u}$ is the external fluid velocity, p is the pressure and μ is the external fluid viscosity. $\boldsymbol{\sigma}$ represents the stress tensor. Inside the capsule, the same equations apply except that the viscosity is multiplied by the viscosity ratio λ.

The partial differential equations, Eqs.(2.1) and (2.2), which are valid in the system volume, are transformed into boundary integral equations valid on the surface of the volume. Based on the standard boundary integral formulation for a capsule freely suspended into the external fluid, the velocity at a point $\boldsymbol{x}_0$ on the capsule interface S_c is determined by the following boundary integral equation(BIE) [32].

$$\begin{aligned} &\boldsymbol{u}(\boldsymbol{x}_0) - 2\boldsymbol{u}^{\infty}(\boldsymbol{x}_0) = \\ &\quad -\frac{1}{4\pi\mu}\int_{S_c} [\boldsymbol{S} \cdot \Delta \boldsymbol{f} - (1-\lambda)\mu \boldsymbol{T} \cdot \boldsymbol{u} \cdot \boldsymbol{n}](\boldsymbol{x})\, dS \end{aligned} \tag{2.3}$$

where $\boldsymbol{u}^{\infty}$ is the flow velocity far from the capsule interface S_c, the tensors $\boldsymbol{S}$ and $\boldsymbol{T}$ are the fundamental solutions for the velocity and stress for the three-dimensional Stokes equations, respectively [33] and are determined using the following equations:

$$S_{ij} = \frac{\delta_{ij}}{r} + \frac{\hat{x}_i \hat{x}_j}{r^3} \tag{2.4}$$

$$T_{ijk} = -6\frac{\hat{x}_i \hat{x}_j \hat{x}_k}{r^5} \tag{2.5}$$

where $\hat{\boldsymbol{x}} = \boldsymbol{x} - \boldsymbol{x_0}$ and $r = |\hat{\boldsymbol{x}}|$. A detailed derivation of BIE may be found in [48].

The dynamics of capsule in the ambient fluid requires specifying boundary conditions on the capsule membrane. At the capsule interface between the external and internal fluid, the velocity $\boldsymbol{u}$ is continuous across the membrane because of the assumption of non-slip and non permeability of the membrane. The hydrodynamic stresses, $\boldsymbol{f} = \boldsymbol{\sigma} \cdot \boldsymbol{n}$, due to the external and the internal fluid flows undergo a discontinuity and are balanced by developing membrane tensions as shown in the following equation:

$$\boldsymbol{u}_1 = \boldsymbol{u}_2 = \boldsymbol{u} \tag{2.6}$$

$$\Delta \boldsymbol{f} \equiv \boldsymbol{n} \cdot (\boldsymbol{\sigma}_2 - \boldsymbol{\sigma}_1) \tag{2.7}$$

The subscripts 1 and 2 are the internal and external fluid, respectively, while $\boldsymbol{n}$ is the unit normal which we choose to point into the external fluid and $\boldsymbol{\sigma}$ is the surface stress tensor. It is of interest to note that the surface stress $\Delta \boldsymbol{f}$ is determined by the membrane dynamics as described in Section 2.2.

Because of the no-slip condition at the capsule interface, the time evolution of any material point on the capsule membrane is determined via the following kinematic condition at the interface:

$$\frac{\partial \boldsymbol{x}}{\partial t} = \boldsymbol{u} \tag{2.8}$$

Although the governing equations and boundary conditions are linear in $\boldsymbol{u}$ and

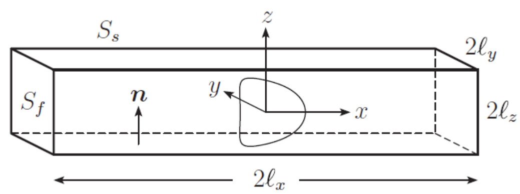

Figure 2.2: Illustration of an elastic capsule flowing at the centerline of a square microchannel [28].

$\boldsymbol{f}$, the problem of determining the capsule shape constitutes a nonlinear problem, i.e., the velocity $\boldsymbol{u}$, and stress $\boldsymbol{f}$ are nonlinear functions of the geometrical variables describing the interface shape [32].

In addition to the three-dimensional elastic capsule suspended in an infinite fluid, the Stokes equations (Eq.2.1) and continuity (Eq.2.2) also represent the typical fluid governing equations in a microfluidic device, where the small length (i.e., micro scale) makes the Reynolds number $Re \leq 1$ and the viscous forces dominant over the inertial ones.

In particular, we consider an elastic capsule with viscosity $\lambda\mu$ flowing in a square microchannel device as shown in Figure 2.2. The fluid external to the capsule has viscosity μ and we assume equal density between the internal and external fluid. The system surface S_B consists of the capsule interface S_c, the microchannel's solid surface S_s, and the fluid surface S_f of the channel's inlet and outlet far from the capsule. The governing equations describing the motion of capsule in a microfluidic device are still Stokes Equation (Eq.2.1) and continuity (Eq.2.2), to which one must add a zero velocity boundary condition. The general boundary integral equation, Eq. 2.3 is then modified to account for the confining boundaries [47] and is found as follows:

$$
\begin{aligned}
\Omega \boldsymbol{u}(\boldsymbol{x}_0) &= -\int_{S_s \cup S_f} [\boldsymbol{S} \cdot \boldsymbol{f_2} - \mu \boldsymbol{T} \cdot \boldsymbol{u_2} \cdot \boldsymbol{n}](\boldsymbol{x})\, dS \\
&\quad - \int_{S_c} [\boldsymbol{S} \cdot \Delta \boldsymbol{f} - (1-\lambda)\mu \boldsymbol{T} \cdot \boldsymbol{u} \cdot \boldsymbol{n}](\boldsymbol{x})\, dS \qquad (2.9)
\end{aligned}
$$

where the subscripts 1 and 2 refer to fluids inside and outside of the capsule, respectively. In the second term on the right-hand side, the velocity is $\boldsymbol{u} = \boldsymbol{u_1} = \boldsymbol{u_2}$. For points $\boldsymbol{x}_0$ on $S_s \cup S_f$, $\Omega = 4(1+\lambda)\mu$ and $\Omega = 4\mu$ for points $\boldsymbol{x}_0$ on the surface S_c.

The dynamics of capsule in the square microchannel device also requires specifying boundary conditions on the capsule membrane. Boundary conditions (Eq.2.6 and (Eq.2.7) described above still apply at the capsule's interface. Additional boundary conditions are specified on microchannel's solid surface S_s and the fluid surface S_f, and are given by

$$
\boldsymbol{u} = 0 \text{ on the solid boundary } S_s, \qquad (2.10)
$$

$$
\boldsymbol{u} = \boldsymbol{u}^\infty \quad \text{or} \quad \boldsymbol{f} = \boldsymbol{f}^\infty \text{ on the fluid surface } S_f \qquad (2.11)
$$

2.2 Membrane Dynamics

A capsule membrane can undergo three different basic modes of deformation: (i) shape-changing deformation(shear), (ii) volume-changing deformation (dilation) and (iii) bending. The capsule membrane dynamics is described using a continuum mechanics approach. Because the membrane thickness is much smaller than the size of capsule, the membrane is treated as a two-dimensional object using the theory of thin shells [48]. In this section, we briefly discuss the membrane dynamics and more details may be found in relevant books [47, 48].

In the absence of fluid inertia, the capsule deformation at any time is governed by a balance between the membrane elastic tensions and the viscous stresses exerted by the flowing fluid. For a membrane with shearing and area-dilation resistance and a negligible bending resistance considered in this work, a force balance over an arbitrary differential area of membrane shows that $\Delta \boldsymbol{f} = -\nabla_s \cdot \boldsymbol{\tau}$ [30], which in contravariant form gives,

$$\Delta \boldsymbol{f} = -(\tau^{\alpha\beta}|_{\alpha}\, \boldsymbol{t}_{\beta} + b_{\alpha\beta}\, \tau^{\alpha\beta}\, \boldsymbol{n}) \tag{2.12}$$

In this expression, $\boldsymbol{\tau}$ is the in-plane stress resultant tensor, $b_{\alpha\beta}$ is the surface curvature tensor, and the $\tau^{\alpha\beta}|_{\alpha}$ notation denotes covariant differentiation. The in-plane stress tensor $\boldsymbol{\tau}$ is derived from the left Cauchy-Green strain tensor and is given by the dyadic product [39].

$$\boldsymbol{\tau} = \sum_{\alpha} \tau_{\alpha}^{P} \hat{\boldsymbol{b}}_{\alpha} \hat{\boldsymbol{b}}_{\alpha} \tag{2.13}$$

The principal elastic tensions τ_{α}^{P} are calculated from the stretch ratios via a constitutive law which depends on the material composition of the membrane [48]. We use the Skalak *etal.* membrane's constitutive law [52] which relates $\tau^{'}$s eigenvalues (or principal elastic tensions $\tau_\beta^P, \beta = 1, 2$) with the principal stretch ratios λ_β by

$$\tau_1^P = \frac{G_s \lambda_1}{\lambda_2}(\lambda_1^2 - 1 + C\lambda_2^2[(\lambda_1\lambda_2)^2 - 1]) \tag{2.14}$$

To determine τ_2^P, reverse the λ_α subscripts. In the equation 2.14, G_s is the membrane shearing modulus while the dimensionless parameter $C \equiv G_a/G_s$ is associated with the area-dilatation modulus G_a of the membrane (scaled with its shearing) [48, 53].

2.3 Membrane Spectral Boundary Element Method

The MSBE is the numerical method used to model and simulate the dynamics of capsule in a microfluidic device. Physical quantities of interest (i.e., $\boldsymbol{u}$ and $\boldsymbol{f}$ are directly computed on the interface. Therefore, there is no need to solve for the fluid flow throughout the whole computational domain in order to capture the dynamics of the membrane. For example, the MSBE algorithm scheme is shown in the Figure 2.3. Given an initial capsule shape, the stretch ratios, λ_α and curvature tensor (local curvature), $b_{\alpha\beta}$ are evaluated. The elastic tensions (local tensions) for Skalak constitutive law are calculated from the stretch ratios using Eq.2.14. The force vector $\Delta\boldsymbol{f}$ is then computed along the capsule surface using Eq.2.12. Eq.(2.9) can be evaluated to solve for the velocity field $\boldsymbol{u}$ on the membrane. The capsule shape equation (the kinematic condition (Eq.2.8) is then used to update the position vector of the membrane material point and calculate the new capsule shape. As a result, this method captures the dynamic evolution of the capsule as the capsule flows inside the microfluidic device.

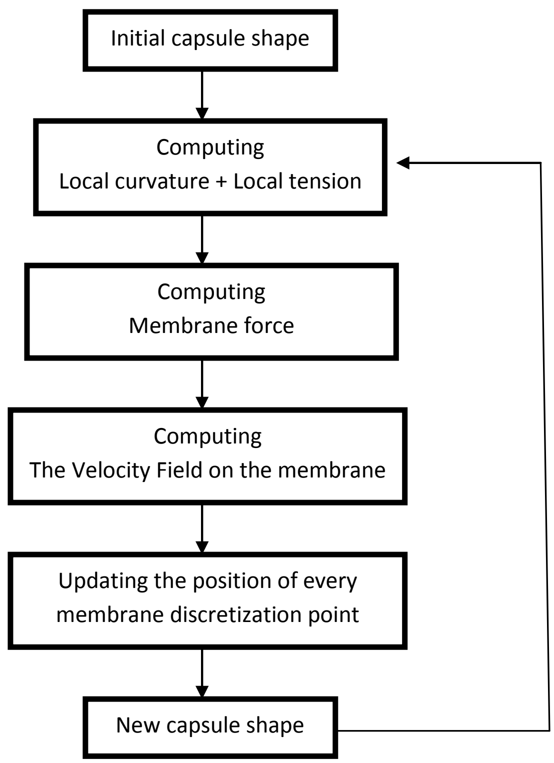

Figure 2.3: Scheme of the Membrane Spectral Boundary Element (MSBE) algorithm used to capture the dynamic evolution of the capsule as it flows inside the microfluidic device.

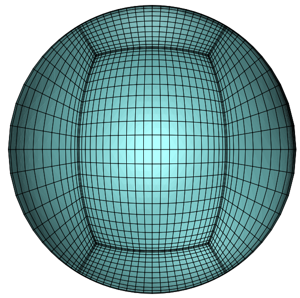

Figure 2.4: The Membrane Spectral Boundary Element (MSBE) discretization of a spherical capsule into $N_E = 6$ elements based on cube projection.

The interested reader is referred to our earlier papers for more details on our MSBE algorithm [30, 32] and our recent investigations on the capsule dynamics in rectangular and constriction microchannels [25, 26].

The discretization used in the MSBE method is a block-structured mesh. In the case of spherical capsule considered in this problem, the initial capsule surface is divided into $N_E \leq 6$ curvilinear quadrilateral elements as illustrated in the Figure 2.4. The MSBE discretization of the spherical capsule is then done via prism projection; e.g. the capsule surface is projected on to a cube whose faces correspond to the interfacial elements as shown in figure 2.4. The surface is discretized in this way so that the distribution of spectral points is controlled on the surface to maximize efficiency and accuracy [32]. The microchannel's solid surface is also discretized using the spectral boundary element. Each quadrilateral surface element is then mapped on to a square parametric domain $[-1, 1]^2$. The geometric variables such as the position of a membrane material point on each element are discretized using Lagrangian interpolation in terms of the parametric variables (ξ, η) on the square domain as follows :

$$\boldsymbol{x}(\xi, \eta) = \sum_{i=1}^{N_B} \sum_{j=1}^{N_B} \boldsymbol{x}(\xi_i, \eta_j) h_i(\xi) h_j(\eta) \tag{2.15}$$

where h_i is the (N_B-1)-order Lagrangian interpolant polynomial. The physical variables $\boldsymbol{u}$ and $\boldsymbol{f}$ are also represented in the same manner as the geometric variables. Since the Lagrangian interpolation guarantees second-order continuity of derivatives, computation of surface properties is easily obtained. For example, first and second derivatives of the position vector are necessary for the evaluation of the stretch ratios, λ_α and curvature tensor, $b_{\alpha\beta}$. The elastic tensions for Skalak constitutive law are calculated from the stretch ratios and the hydrodynamic traction (or the surface stress vector), $\boldsymbol{f}$ is then computed using Eq.2.12.

The base points (ξ_i, η_j) for the interpolation are chosen as the zeros of N_B-order orthogonal polynomials. The boundary integral equation (2.9) admit two different types of points, the collocation points $\boldsymbol{x_0}$ of the left-hand side where the equation is required to hold and the basis points $\boldsymbol{x}$ of the right-hand side where the physical variables $\boldsymbol{u}$ and $\boldsymbol{f}$ are defined. The spectral element method use collocation points of Gauss quadrature, i.e., in the interior of the element only. As a result, the boundary integral equation holds even for singular elements where the normal vector is not uniquely defined, i.e., the elements which contain the corners of the microfluidic channel. In addition, we use basis points $\boldsymbol{x}$ of Gauss-Lobatto quadrature (i.e., in the interior and the edges of the elements). Therefore, the physical variables are determined in the interior and on the edges of the spectral elements. The numerical integration associated with Eq.2.9 is performed by Gauss-Legendre quadrature with the aid of variable transformations [30, 32].

Using the kinematic condition (2.8), we determine the capsule's shape as a function of time. This is based on a high-order explicit scheme , i.e., the fourth-order Runge-Kutta method. We note that the interfacial velocity $\boldsymbol{u}$ has both normal and tangential velocity components and the grid points represent membrane material points of the capsule's interface. The explicit time integration is applied at the (Gauss-Lobatto) basis points $\boldsymbol{x}$ where the interfacial velocity $\boldsymbol{u}$ is determined. We emphasize that the time step Δt should be sufficiently small to ensure numerical stability [30, 32], i.e.,

$$\Delta t < O(Ca \Delta x_{min}) \tag{2.16}$$

where Δx_{min} is the minimum length scale appearing in the computational problem, e.g. the minimum grid spacing.

Chapter 3: Dynamics of an elastic capsule in a microfluidic cross-junction

3.1 Problem description

Here, we consider a three-dimensional capsule suspended into another liquid (thus subjected to hydrodynamic forces) and flowing along the centerline of a microfluidic cross-junction as illustrated in Figure 3.1. Its deformation is measured as a displacement from the reference shape that is assumed to be spherical. The cross-junction is constructed from two intersecting square microfluidic channels with cross-section half lengths $\ell_y = \ell_z$. The origin of the co-ordinate system is placed at the center of the junction. We think of one channel as horizontal and the other as vertical as illustrated in Figure 3.1. At time $t = 0$, the capsule is located upstream of the cross-junction in the horizontal channel and has a spherical shape with radius a and centroid $x_c = -4\ell_z$. That instant, the flow is turned on inside of the microfluidic device and we investigate the transient dynamics of the capsule as it enters and exits the microfluidic cross-junction which occupies the x-region [-ℓ_z, ℓ_z].

The capsule's interior and exterior fluids are Newtonian fluids, with viscosities $\lambda\mu$ and μ, and have equal density (i.e., no buoyancy and sedimentation effects). We

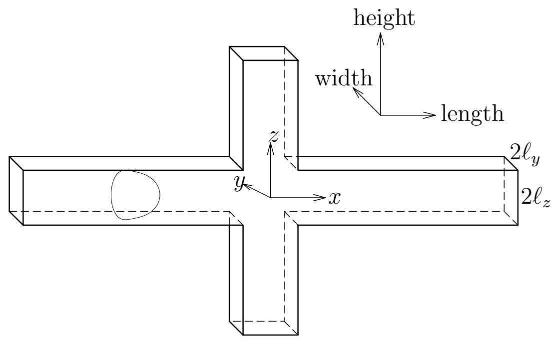

Figure 3.1: Illustration of an elastic capsule flowing at the centerline of a microfluidic cross junction.

define the capsule size by $a = (3V/4\pi)^{1/3}$ where V is the capsule volume. It is important to assume that the capsule has a negligible membrane permeability(i.e., no flow through the membrane) and its volume is constant. At the inlet upstream of the cross-junction in the horizontal channel, a velocity flow profile is imposed as well as no-slip and no penetration boundary conditions are imposed on solid walls. Far from the capsule, the flow approaches the undisturbed flow $\boldsymbol{u}^{\infty}$ in a channel characterized by a constant flow rate $Q = 4\mathcal{U}\ell_z^2$. The exact form of the channel's velocity field $\boldsymbol{u}^{\infty}$ which is described below and its average velocity $\mathcal{U}$ is given in Section 2 of our recent paper on capsule motion in a square microfluidic channel [27].

$$\frac{u_x^{\infty}}{\Upsilon} = (\ell_z^2 - z^2) + \sum_{m=1}^{\infty} B_m \cosh\left(\frac{b_m y}{\ell_z}\right) \cos\left(\frac{b_m z}{\ell_z}\right) \tag{3.1}$$

where

$$\Upsilon = -\frac{1}{2\mu}\frac{dp}{dx}, \quad b_m = \frac{(2m-1)\pi}{2}, \qquad B_m = \frac{(-1)^m 4\ell_z^2}{b_m^3 \cosh\left(\frac{b_m \ell_y}{\ell_z}\right)}, \tag{3.2}$$

where p is the dynamic pressure.

To compute the volumetric flow rate Q over the cross-section area, we integrate Eq. (3.1)

$$\frac{Q}{\Upsilon} = \frac{8\ell_y \ell_z^3}{3} + \sum_{m=1}^{\infty} B_m \left(\frac{2\ell_z}{b_m}\right)^2 \sinh\left(\frac{b_m \ell_y}{\ell_z}\right) \sin(b_m) \tag{3.3}$$

The average velocity of the exterior fluid far from the capsule is $\mathcal{U} = Q/(\ell_z^2)$ The capsule velocity in the flow direction U_x may be different than the average velocity $\mathcal{U}$ in the horizontal channel. The incoming flow rate at each of the two inlets of the vertical microchannel is defined as Q_v. After the cross-junction, the horizontal channel has a total constant flow rate of $(Q + 2Q_v)$. We assume that the Reynolds-number is small for both the surrounding and the inner flows, thus the capsule deformation and motion occur in the Stokes regime.

Furthermore, we consider a slightly over-inflated capsule made from a thin strain-hardening elastic membrane obeying the Skalak *etal.* constitutive law [52] with comparable shearing and area-dilatation resistance. This capsule is called Skalak capsule in this thesis. Due to osmotic effects and a positive osmotic pressure difference p^0 between the capsule's interior and exterior fluids often encountered during the fabrication of artificial capsules [17], the capsule membrane in our work is prestressed (over-inflated) by an isotropic elastic tension to account for the osmotic effects [6] and prevent buckling instabilities [28]. To add the capsule over-inflation, we define the prestress parameter α_p such that all lengths in the undeformed capsule would be scaled by $(1 + \alpha_p)$, relative to the reference shape [25]. Since the capsule is initially spherical, its membrane is initially prestressed by an isotropic elastic tension

$\tau_0 = \tau^P_\beta(t = 0)$ which depends on the employed constitutive law and its parameters but not on the capsule size. For example, given a Skalak capsule with membrane hardness $C = 1$ and prestress $\alpha_p = 0.05$ considered in this problem, the undisturbed capsule size is 5 % higher than that of the reference shape and the initial membrane tension due to prestress is $\tau/G_s \approx 0.3401$. The capsule motion and deformation depend on four additional dimensionless parameters: the capsule size (relative to the channel height) a/ℓ_z, the relative lateral flow rate Q_v/Q, the viscosity ratio λ, and the capillary number Ca defined as

$$\mathrm{Ca} = \frac{\mu \mathcal{U}}{G_s} \tag{3.4}$$

where $\mathcal{U}$ is the average flow velocity in the upstream horizontal channel before the cross-junction.

First, we investigate the transient dynamics of low viscosity capsules (i.e., for viscosity ratio $\lambda = 0.01$) with different sizes, flow rate and lateral flow rates. We then investigate the transient dynamics of equiviscous capsules (i.e., for viscosity ratio $\lambda = 1$) and compare results of capsules with different viscosity ratio. Note that the capillary number, as defined by Eq. 3.4, does not contain any length scale and thus it may be considered as a dimensionless flow rate. In this study, the channel's half-height ℓ_z is used as the length scale,the velocity is scaled with the average undisturbed velocity $\mathcal{U}$ of the upstream horizontal channel, and thus the time scale is $\tau_f = \ell_z/\mathcal{U}$. For a fixed capsule size a/ℓ_z, varying the capillary number Ca can be achieved in an experiment by keeping the exterior-fluid viscosity and lateral flows fixed and varying the flow rate Q, or average velocity $\mathcal{U}$. Similarly, for a fixed capillary number Ca,and viscosity ratio, varying the capsule size a/ℓ_z can be achieved by keeping lateral flows fixed and using different volumes of capsules from the same membrane (and with the same prestress level). For a fixed capsule size a/ℓ_z and capillary number Ca, varying the the viscosity ratio λ can easily be achieved in an experiment by varying the external-fluid viscosity.

The capsule deformation is defined through the capsule's dimensions (i.e., capsule projection lengths along the three axes, L_x, L_y, and L_z) and profile curvatures. The profile curvatures are determined along the capsule's $y = 0$ profile (i.e., the cross section of the capsule surface with the $y = 0$ plane). In addition, we calculate curvatures at the downstream and upstream edges of the capsule (i.e., its intersections with the x axis). As the capsule moves in the channel, its volume-average velocity is determined by,

$$U = \frac{1}{V}\int_V \boldsymbol{u}\, dV = \frac{1}{V}\int_{S_c} \boldsymbol{u}\cdot\boldsymbol{n}\, dS \tag{3.5}$$

3.2 Dynamics of low-viscosity capsule in a cross-junction microchannel

In this section, we present our results by considering the transient deformation of a low-viscosity capsule with size $a/\ell_z = 0.9$, viscosity ratio $\lambda = 0.01$, capillary number Ca $= 0.05$, and relative lateral flow $Q_v/Q = 1.5$ as it deforms inside the cross-junction microfluidic device. Our focus is on the transient behavior of the low-viscosity capsule as it enters and exits the cross-junction. Different capsule shape transitions are shown in Figure 3.2 as the capsule flows inside the microfluidic cross-junction device. Some of these shapes are in agreement with previous studies of capsule dynamics in axisymmetric-like solid ducts such as cylindrical and square microchannels where capsules obtain steady-state bullet-like and parachute-like shapes, elongated along the flow direction [4, 5, 26, 28]. However, the asymmetric shape of our cross-junction gives rise to capsule shapes not observed in neither cylindrical nor square microchannels. Just before the cross-junction entrance (i.e., $x_c/\ell_z = -1.50$), the capsule obtains a bullet-like shape. This is a typical capsule shape observed in axisymmetric-like solid ducts. When the capsule is inside the cross-junction (i.e., $x_c/\ell_z = -0.07$), its initially bullet-like shape becomes pointed and elongated in the flow direction due to deforming hydrodynamic forces caused by intersecting vertical flows. In this case, it is important to note that in order to balance the strong deforming hydrodynamics forces, the capsule tries to increase its downstream curvature while its upstream curvature decreases so that its total restoring tension force on the membrane is increased. This deformation, identified in our earlier studies of capsule dynamics in planar extensional flows or square channels, results from the curvature term in the membrane traction, eqn 2.12 [21, 22, 28]. While the capsule is still inside the cross-junction (i.e., its centroid is nearly at $a/\ell_z = 0.85$), the increased hydrodynamic forces from the incoming vertical flows cause the capsule to obtain a cylindrical-like shape. The capsule is now elongated along the flow direction as shown in Figure 3.2 (a) and (b). This shape reveals that the intersecting flows from the vertical channels at the cross-junction act like a

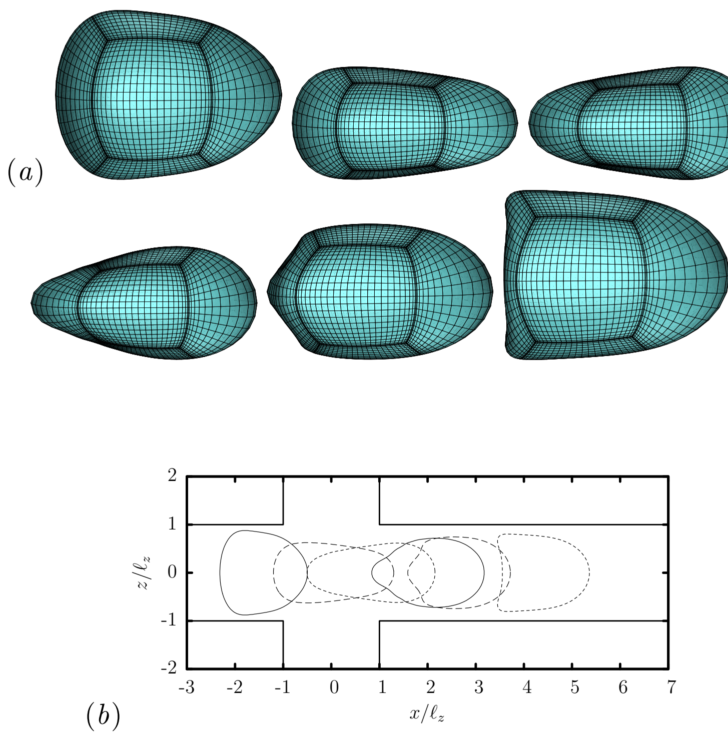

Figure 3.2: The shape of a capsule (plotted row-wise) with $a/\ell_z = 0.9$, $\lambda = 0.01$, $\mathrm{Ca} = 0.05$, and $Q_v/Q = 1.5$ inside the microfluidic device as seen from (a) the negative y-axis (i.e., front view) at centroid $x_c/\ell_z = -1.50, -0.07, 0.85, 1.42, 2.58, 4.18$. ($b$) As in ($a$) but for capsule profile (i.e., capsule intersection with the plane y=0).

constriction, and thus the capsule needs to be compressed inside of the constriction. At $x_c/\ell_z = 1.42$, as the capsule exits the cross-junction while its rear is still inside the cross-junction, the capsule has an inverse bullet-like shape (i.e., its front edge curvature becomes rounded while its rear edge curvature is pointed). The explanation is straightforward if we consider the fast incoming vertical flows, the capsule at this point moves slower than the surrounding fluid which flows in the positive horizontal direction (i.e., toward downstream of the cross-junction), and at this location the capsule needs to obtain an inverse bullet-like shape for hydrodynamic stability reasons. At $x_c/\ell_z = 2.58$, the capsule obtains a more pointed tail rear in response to the increased hydrodynamic forces from intersecting vertical flows. To explain the pointed tail developed at the capsule rear, we need to consider the interaction of the hydrodynamic forces with the membrane tensions. It is important to note that the restoring membrane tensions (which are required to balance the deforming hydrodynamic forces) result from both the local tension and the local curvature, e.g. the curvature term in eq.2.12. After the cross-junction, the restoring membrane tensions become weaker in response to the stronger hydrodynamic forces. Therefore, the capsule needs to increase the rear tail curvature significantly to produce a strong enough local interfacial force. We plot the evolution of downstream and upstream edge curvatures as function of the centroid x_c in Figure 3.3. Note that both C_{xz} and C_{xy} are line curvatures, determined along the interfacial cross-section with the planes $y = 0$ and $z = 0$ respectively. Observe that inside the cross-junction (i.e., $x_c/\ell_z = -0.07$), the upstream edge curvature, C^u_{xz} shows a monotonic increase owning to the stronger hydrodynamic forces from the intersecting vertical flows and that the maximum value of the edge curvature, C^u_{xz}, is around $x_c/\ell_z = 1.42$ just when the capsule rear exits the cross-junction; thus it is during this location that the capsule develops a pointed rear tail. The capsule becomes much more pointed at $x_c/\ell_z = 2.58$ when the capsule rear is out of the cross-junction.

At $x_c/\ell_z = 4.18$ far downstream of the cross-junction, the two rear curvatures, C^u_{xz} and C^u_{xy} are equal and the tail gradually disappears as the capsule obtains the parachute-like shape. On the other hand, the downstream edge curvatures, C^d_{xz} and C^d_{xy} show a fast initial increase before the cross-junction followed by a similarly fast decrease inside the cross-junction (even though $C^u_{xz} > C^u_{xy}$). These two front curvatures remain nearly equal as the capsule passes through the cross-junction and develops a rear tail. Far downstream of the cross-junction at $x_c/\ell_z = 4.18$, the increased flow rate (i.e., the increased local capillary number $\mathrm{Ca}^{eff} = \frac{2\mu\mathcal{U}}{G_s} = 2\mathrm{Ca}$) causes the capsule to obtain a parachute-like shape. The overall capsule deformation inside the microfluidic cross-junction can also be observed from the evolution of capsule profiles with the plane $y = 0$, shown in Figure 3.2(b). It is of interest to note that the pointed rear tail around $x_c/\ell_z = 1.42$ and $x_c/\ell_z = 2.58$ is similar to the pointed spindled shape of capsule obtained in extensional flows so that they are able to withstand increased flow rates [21].

3.2.1 Effects of capsule size

To investigate more the tail formation of low-viscosity capsule, we study the effects of the capsule size inside the microfluidic cross-junction device. In particular,

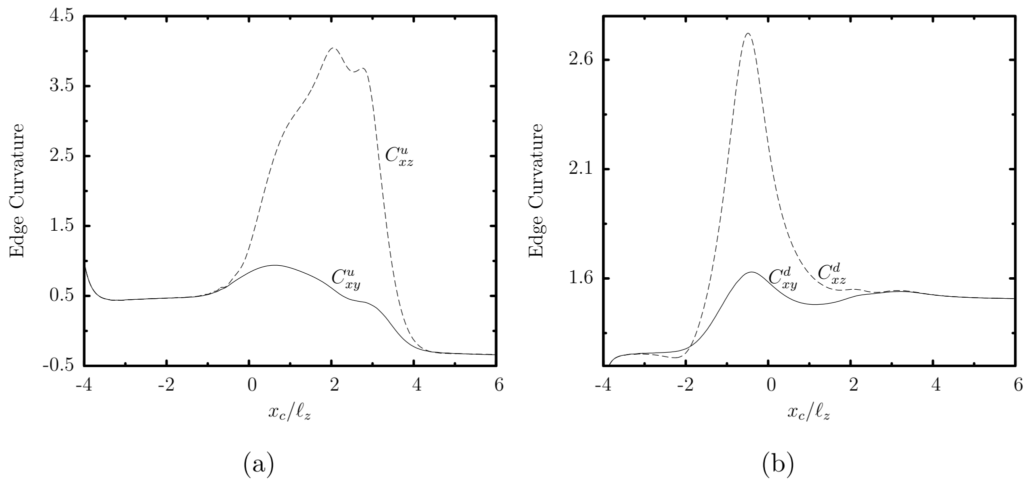

Figure 3.3: Evolution of capsule properties as a function of the centroid x_c, for a capsule with Ca $= 0.05$, $\lambda = 0.01$, $Q_v/Q = 1.5$ and $a/\ell_z = 0.9$. (a) Curvatures C^u_{xz} and C^u_{xy} at the capsule's upstream edge. (b) Curvatures C^d_{xz} and C^d_{xy} at the capsule's downstream edge. The Curvatures are scaled with the curvature of the undisturbed spherical shape.

we consider capsules with $Ca = 0.1$, $\lambda = 0.01$, $Q_v/Q = 0.5$ and investigate its transient dynamics for various capsule size i.e., $a/\ell_z = 0.7, 0.8, 0.9$. We analyze our results by looking at capsule geometrical properties (i.e., capsule's dimensions and profile curvatures) and capsule velocity U_x as shown in Figure 3.4. As the capsule size increases (thus higher flow blocking), the stronger hydrodynamic forces cause a significant capsule deformation, i.e., the capsule length L_x increases while its height L_z decreases significantly as illustrated in the Figure 3.4 (a) and (b). The hydrodynamic flow forces are stronger owning to the smaller gap between the capsule interface and the solid walls, and cause the capsule to deform into a bullet-like shape before the cross-junction. When the capsule enters the cross-junction, the stronger hydrodynamic forces owing now to the intersecting vertical channels cause a remarkable capsule elongation. The capsule continues to elongate as it exits the cross-junction, achieving its highest elongation approximately near $x_c/\ell_z = 1.5$ for the larger capsule studied (i.e., $a/\ell_z = 0.9$). In a similar manner, the capsule's height L_z decreases significantly when the capsule is inside the cross-junction to accommodate for the stronger hydrodynamic forces as shown in Figure 3.4 (b). Figure 3.4 (d) shows the capsule profile (i.e., capsule intersection with the plane y = 0) just after the cross-junction at $x_c/\ell_z = 2.13$. It is important to observe that as the capsule size increases, the capsule develops a pointed rear tail owning to the increased hydrodynamic forces from both the fast incoming vertical flows and the narrower gap between the capsule interface and the channel walls.

As the capsule size increases, the narrower gap between the capsule interface and the channel walls results in a reduction of the capsule velocity. Thus, larger capsules take more time to pass the cross-junction. Figure 3.4 (c) shows the evolution of capsule velocity U_x inside the cross- junction. To understand how the capsule velocity U_x varies with capsule size, we use the scaling analysis developed for capsule motion in a square channel [27]. It is important to emphasize that our earlier analysis was valid for steady-state capsule motion in straight solid ducts such as cylindrical, square or rectangular channels. However, if we consider our current problem over the entire horizontal channel, the capsule dynamics inside the cross-junction is similar to the dynamics in a straight solid ducts (i.e., the capsule obtains similar steady-state bullet-like and parachute-like shapes, elongated along the flow direction). Furthermore, our problem occurs in the Stokes regime; thus we further apply the quasi-steady nature of the Stokes flow in the analysis. Using Eqn (19) from our previous investigation of capsule dynamics in square channel [27], the capsule

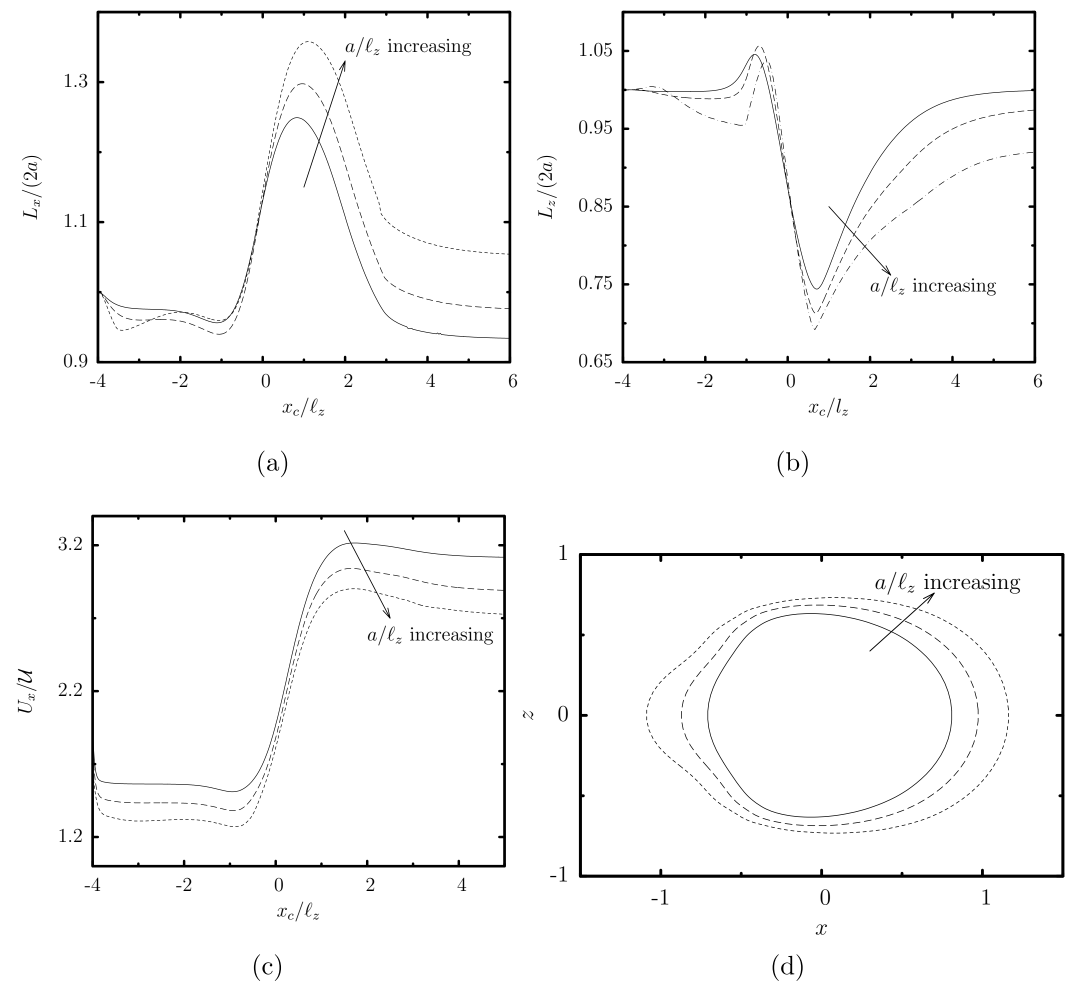

Figure 3.4: Evolution of capsule properties as a function of the centroid x_c, for a capsule with Ca $= 0.1$, $\lambda = 0.01$, $Q_v/Q = 0.5$ and size $a/\ell_z = 0.7, 0.8, 0.9$. (a) Length L_x, and (b) height L_z of the capsule (scaled with the length $2a$ of the undisturbed spherical shape). These lengths are determined as the maximum distance of the interface in the x, y and z directions.(c) Capsule velocity U_x (scaled with the average undisturbed velocity $\mathcal{U}$ of the upstream horizontal channel). (d) Capsule profile (i.e., capsule intersection with the plane y=0) just after the cross-junction at $x_c/\ell_z = 2.13$ for $a/\ell_z = 0.7, 0.8, 0.9$.

velocity inside the cross-junction should scale proportionally with the gap h between the capsule surface and the solid walls,

$$\frac{U_x - \mathcal{U}}{\mathcal{U}} \sim \frac{h}{\ell_z} \tag{3.6}$$

where $\mathcal{U}$ is the average undisturbed velocity in the horizontal channel), note that Eqn 3.6 represents only qualitatively the present problem by considering the gap h between the capsule surface and the solid walls in the xz-plane where the strongest hydrodynamic forces occur owing to the intersecting vertical flows. As the capsule size a/ℓ_z increases, the gap h between the capsule surface and the solid walls decreases, and thus the capsule velocity decreases, in agreement with our computational results shown in Figure 3.4 (c)

3.2.2 Effects of flow rate

We now investigate the effects of flow rate on the capsule deformation and tail formation. In particular, we consider capsules with $a/\ell_z = 0.9$, $\lambda = 0.01$, $Q_v/Q = 0.5$ and investigate its transient dynamics for $\mathrm{Ca} = 0.05, 0.1$. Figure 3.5 shows the evolution of the capsule properties as a function of the centroid x_c. We note that the effects of decreasing the flow rate Ca for a given fixed capsule size are similar to those of increasing the capsule size a for a given fixed flow rate discussed earlier in section 3.2.1, since both effects result in a higher flow blocking with the flow rate effects due to the reduced interfacial deformation. As Ca increases, the thickness h of the lubrication film between the capsule interface and the channel walls increases, thus reducing the strong local lubrication forces in the flow direction. The capsule appears like a bullet. Inside the cross-junction, the capsule's length L_x increases while its height L_z decreases owning to the stronger hydrodynamic forces. This causes the capsule to extend along the flow direction for interfacial stability. After the cross-junction, the increased flow rate causes the capsule to obtain a more pointed rear tail as shown in the Figure 3.5 (d). Note that the capsule velocity U_x increases as Ca increases because the flow blocking is reduced as a result of the increase in the thickness h of the lubrication film.

3.2.3 Effects of lateral flows

The effects of the lateral flow rates on the capsule dimensions and profiles are presented in Figure 3.6. For a given fixed flow rate Ca $= 0.05$, $\lambda = 0.01$, $a/\ell_z = 0.9$, increasing lateral flow rates (thus stronger hydrodynamic forces) causes a significant change in the capsule's overall shape, i.e., capsule's length L_x increases significantly while its height L_z decreases as shown in Figure 3.6 (a) and (b). The capsule profiles presented in Figure 3.6 (d) show that higher lateral flow rates result in the development of a pointed rear tail just after the capsule exits the cross-junction (i.e., at $x_c/\ell_z = 2$). To explain the evolution of the pointed rear tail, we consider again the interaction between the hydrodynamic forces with the membrane tensions. As the lateral flow rates increase, the stronger hydrodynamic forces owning to increasing lateral flows overcome the weak membrane tensions and thus the capsule needs to increase the tail curvature significantly to produce strong enough local

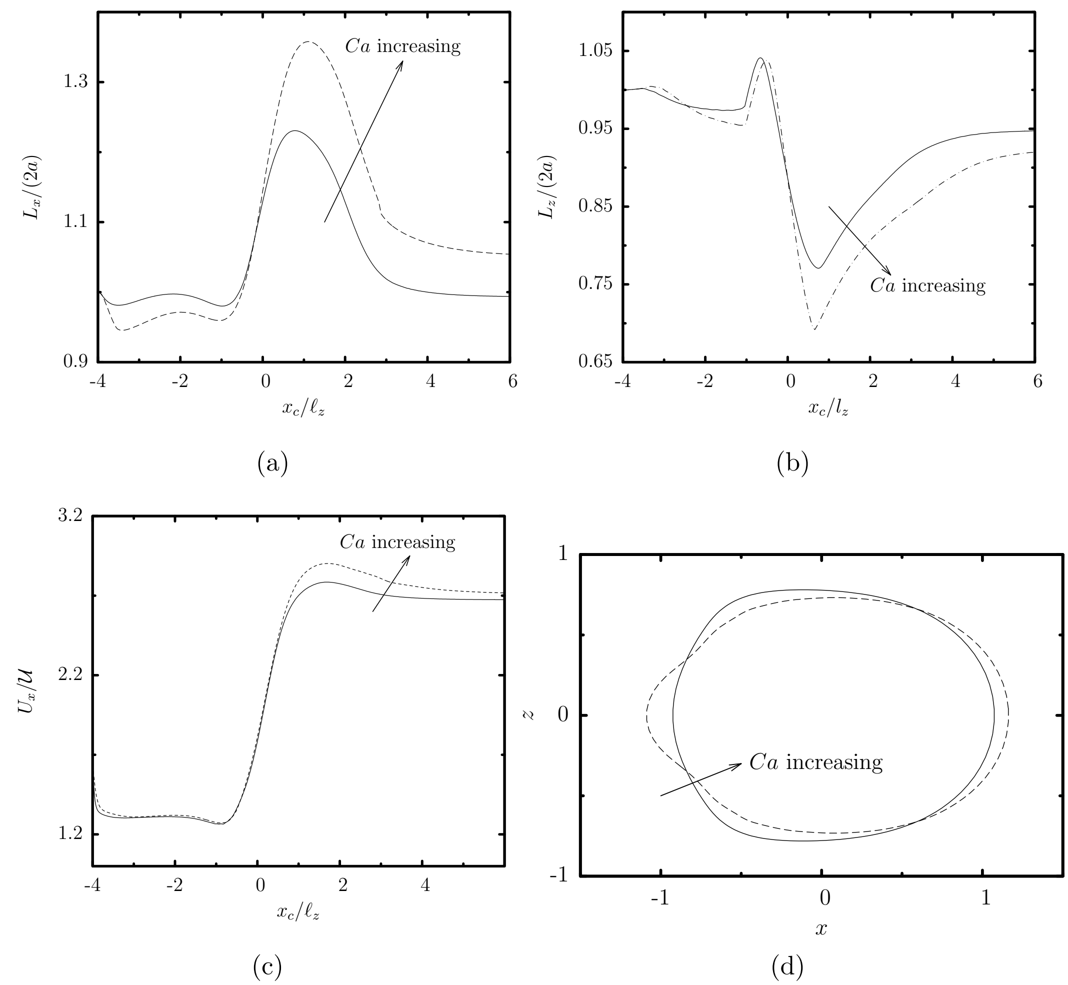

Figure 3.5: Evolution of capsule properties as a function of the centroid x_c, for a capsule with $a/\ell_z = 0.9$, $\lambda = 0.01$, $Q_v/Q = 0.5$ and capillary number $\mathrm{Ca} = 0.05, 0.1$. (a) Length L_x, and (b) height L_z of the capsule (scaled with the length $2a$ of the undisturbed spherical shape).These lengths are determined as the maximum distance of the interface in the x, y and z directions (c) Capsule velocity U_x (scaled with the average undisturbed velocity $\mathcal{U}$ of the upstream horizontal channel). (d) Capsule profile (i.e., capsule intersection with the plane y=0) just after the cross-junction at $x_c/\ell_z = 2.13$ for $\mathrm{Ca} = 0.05, 0.1$.

interfacial forces. After some time, far downstream of the cross-junction, the membrane tensions increases, the tail gradually disappears, and the capsule obtains its steady-state parachute-like shape. As the lateral flow rates increase, the capsule velocity increases as depicted in Figure 3.6(c) since the average fluid velocity in the horizontal square channel after the cross-junction is increased.

3.3 Dynamics of equiviscous capsule in a cross-junction microchannel

In this section, we present our results by considering the transient deformation of an equiviscous capsule with size $a/\ell_z = 0.9$, viscosity ratio $\lambda = 1$, capillary number $\mathrm{Ca} = 0.05$, and relative lateral flow $Q_v/Q = 1.5$ as it deforms inside the cross-junction microfluidic device. Note that the overall capsule transient dynamics for viscosity ratio $\lambda = 1$ is similar to that described for capsules with $\lambda = 0.01$ in Section 3.2. The equiviscous capsule dynamics and deformation result in the different dynamic shape transitions from elongated bullet-like to highly non-axisymmetric three-dimensional shapes as shown in the Figure 3.7. Just before entering the cross-junction, the capsule obtains a bullet-like shape. When the capsule is inside the cross-junction (i.e., $x_c/\ell_z = -0.07$), its initially bullet-like shape becomes pointed and elongated in the flow direction due to deforming hydrodynamic forces caused by intersecting vertical flows.

As the capsule exits the cross-junction (i.e., its centroid is nearly at $a/\ell_z = 0.85$), the increased hydrodynamic forces from the fast incoming vertical flows cause

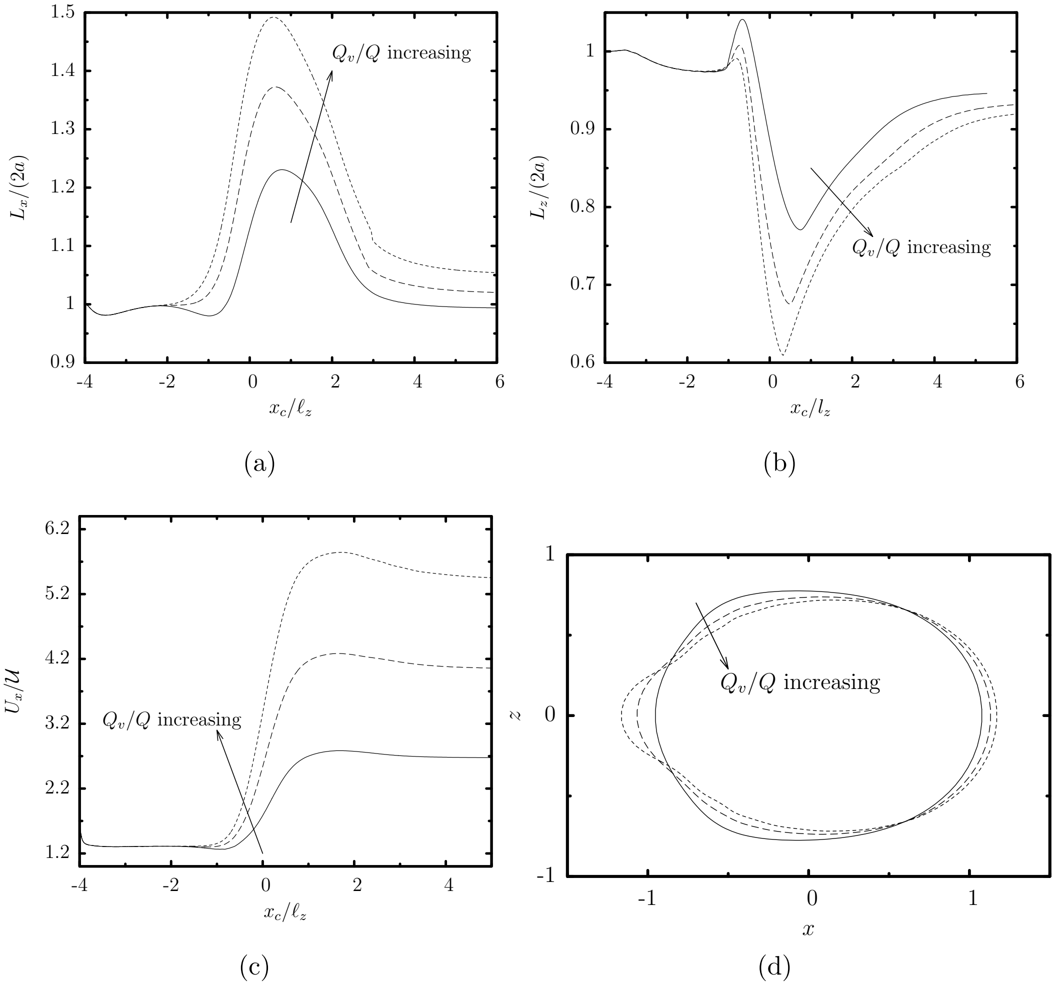

Figure 3.6: Evolution of capsule properties as a function of the centroid x_c, for a capsule with $a/\ell_z = 0.9$, $\lambda = 0.01$, $\mathrm{Ca} = 0.05$ and lateral flows $Q_v/Q = 0.5, 1.0, 1.5$. (a) Length L_x, and (b) height L_z of the capsule (scaled with the length $2a$ of the undisturbed spherical shape). (c) Capsule velocity U_x (scaled with the average undisturbed velocity $\mathcal{U}$ of the upstream horizontal channel). (d) Capsule profile (i.e., capsule intersection with the plane y=0) just after the cross-junction at $x_v/\ell_z = 2$ for $Q_v/Q = 0.5, 1.0, 1.5$.

the capsule to elongate along the flow direction as seen in Figure 3.7 (a) and (b). The intersecting flows from the vertical channels act like a constriction, thus the capsule is compressed inside the cross-junction. At the capsule centroid $x_c/\ell_z = 1.42$, as the capsule exits the cross-junction while its rear is inside the cross-junction, the capsule has an inverse bullet-like shape. When the capsule moves further downstream while its rear exits the cross-junction, the capsule downstream edge becomes more rounded and it is its rear which is now pointed in response to the increased hydrodynamic forces from intersecting lateral flows, as seen in Figure 3.7 (a) and (b) for $x_c/\ell_z = 2.58$. We explain the rear tail formation via the evolution of downstream and upstream edge curvatures shown in Figure 3.8. Note that the restoring membrane tensions result from both the local tension and the local curvature, as seen in Eq.2.12. Since the restoring membrane tensions become weaker than the stronger hydrodynamic forces, the capsule increases the rear tail curvature significantly to produce a strong enough local interfacial force. Inside the cross-junction (i.e., $x_c/\ell_z = -0.07$), C^u_{xz} shows a monotonic increase owning to the stronger hydrodynamic forces from the intersecting vertical flows and reaches a maximum value around $x_c/\ell_z \approx 2$ just when the capsule rear is out of the cross-junction. It is during this location that the capsule produces a strong local interfacial force, thus develops a pointed rear tail for interfacial stability reasons. Observe that the two rear curvatures, C^u_{xz} and C^u_{xy} are equal far downstream of the cross-junction (i.e., $x_c/\ell_z = 4.18$) and the tail gradually disappears as the capsule obtains the steady-state bullet-like shape. The downstream edge curvatures, C^d_{xz} and C^d_{xy} show a fast initial increase before the cross-junction followed by a similarly fast decrease inside

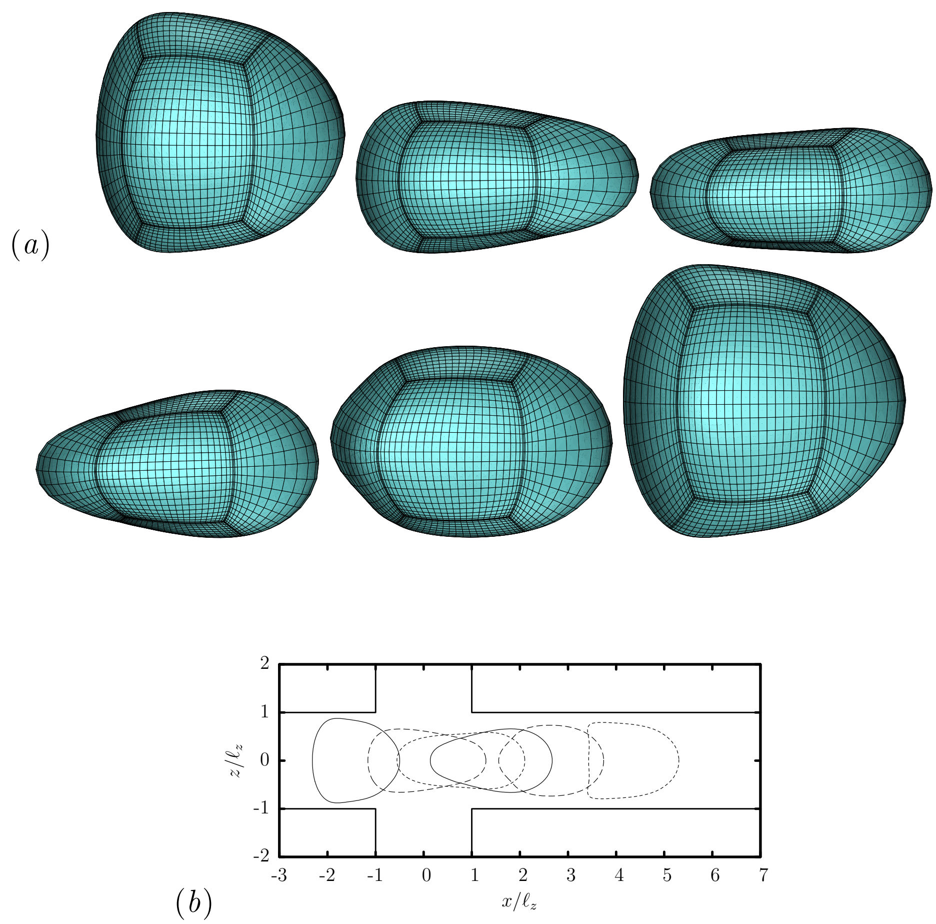

Figure 3.7: The shape of a capsule (plotted row-wise) with $a/\ell_z = 0.9$, $\lambda = 1$, Ca $=$ 0.05, and $Q_v/Q = 1.5$ inside the microfluidic device as seen from (a) the negative y-axis (i.e., front view) at centroid $x_c/\ell_z = -1.50, -0.07, 0.85, 1.42, 2.58, 4.18$. ($b$) As in ($a$) but for capsule profile (i.e., capsule intersection with the plane y=0).

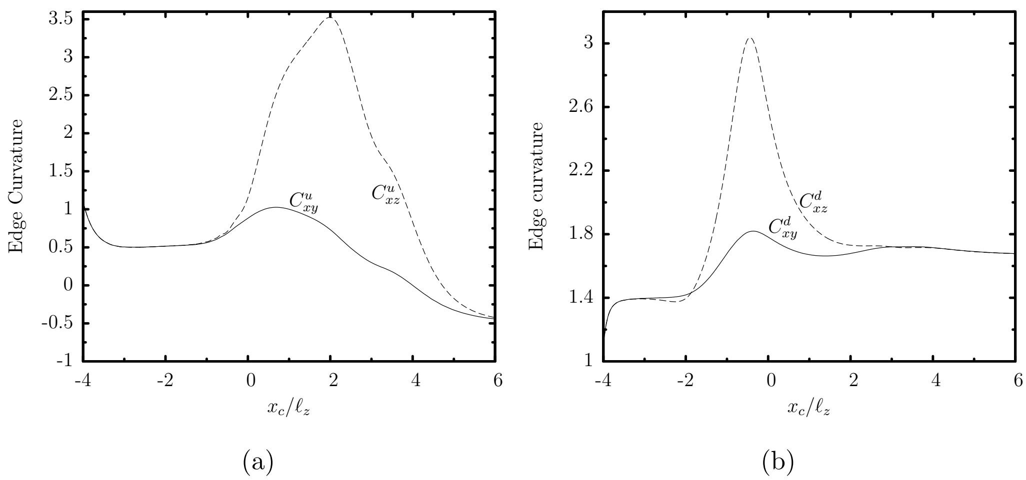

Figure 3.8: Evolution of capsule properties as a function of the centroid x_c, for a capsule with $\mathrm{Ca} = 0.05$, $\lambda = 1$, $Q_v/Q = 1.5$ and $a/\ell_z = 0.9$. (a) Curvatures C^d_{xz} and C^d_{xy} at the capsule's downstream edge. (b) Curvatures C^u_{xz} and C^u_{xy} at the capsule's upstream edge. The Curvatures are scaled with the curvature of the undisturbed spherical shape.

the junction as seen in Figure 3.8 (a). These two front curvatures remain nearly equal as the capsule passes through the cross-junction and develops a rear tail. Far downstream of the cross-junction at $x_c/\ell_z = 4.18$, the increased flow rate (i.e., the increased local capillary number $\mathrm{Ca}^{eff} = \frac{2\mu\mathcal{U}}{G_s} = 2\mathrm{Ca}$) causes the capsule to obtain a bullet-like shape.

3.3.1 Effects of size

In the present section, we study the effects of the capsule size inside the microfluidic cross-junction device. In particular, we consider capsules with $Ca = 0.1$, $\lambda = 1$, $Q_v/Q = 0.5$ and investigate its transient dynamics for various capsule sizes i.e., $a/\ell_z = 0.7, 0.8, 0.9$. As the capsule size increases (thus higher flow blocking), the stronger hydrodynamic forces cause a significant capsule deformation, i.e., the capsule length L_x increases while its height L_z decreases significantly as seen in Figure 3.9 (a) and (b). Capsule profiles are shown in the Figure 3.9 (d) for $x_c/\ell_z = 2.13$. Note that as the capsule size increases, the capsule develops a rounded rear owning to the increased hydrodynamic forces from both the fast incoming lateral flows and the narrower gap between the capsule interface and the channel walls. In addition, the capsule velocity decreases owning to higher flow blocking caused by the narrower gap between the capsule interface and the channel walls. Thus, larger capsules take more time to pass through the cross-junction in agreement with Eq.3.6 and our computational finding shown in Figure 3.9 (c).

3.3.2 Effects of flow rate

In this section, we present the effects of flow rates on the capsule deformation and tail formation. In particular, we consider capsules with $a/\ell_z = 0.9$, $\lambda = 1$,$Q_v/Q = 0.5$ and investigate its transient dynamics for $\mathrm{Ca} = 0.05, 0.1$. We also note that the effects of decreasing the flow rate Ca for a given fixed capsule size are similar to those of increasing the capsule size a for a given fixed flow rate discussed earlier in section 3.3.1, since both effects result in a higher flow blocking with the former due to the reduced interfacial deformation. Figure 3.10 (a) and (b) shows the evolution of the capsule properties. As Ca increases, the capsule's length L_x increases while its height L_z decreases owning to the stronger hydrodynamic forces. This results in a rich deformation of capsule and development of a pointed rear tail as seen in Figure 3.10 (d). In addition, the capsule velocity U_x increases

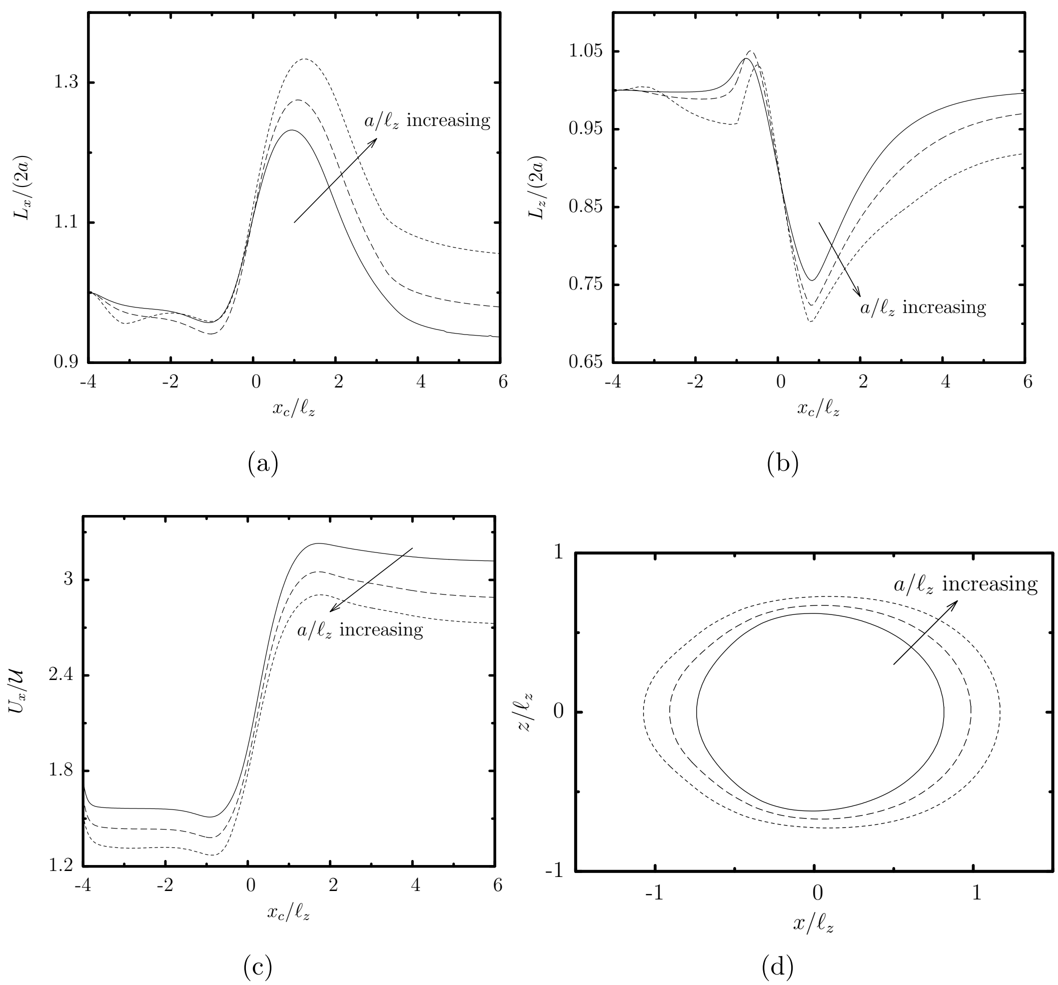

Figure 3.9: Evolution of capsule properties as a function of the centroid x_c, for a capsule with $\mathrm{Ca} = 0.1$, $\lambda = 1$, $Q_v/Q = 0.5$ and size $a/\ell_z = 0.7, 0.8, 0.9$. (a) Length L_x, and (b) height L_z of the capsule (scaled with the length $2a$ of the undisturbed spherical shape). (c) Capsule velocity U_x (scaled with the average undisturbed velocity $\mathcal{U}$ of the upstream horizontal channel). (d) Capsule profile (i.e., capsule intersection with the plane y=0) just after the cross-junction at $x_c/\ell_z = 2.13$ for $a/\ell_z = 0.7, 0.8, 0.9$.

as Ca increases because the flow blocking is reduced as a result of the increase in the thickness h of the lubrication film between the capsule interface and the channel walls. As the capsule deformation increases owning to higher effective Ca, it moves faster inside the cross-junction as seen in Figure 3.10 (c).

3.3.3 Effects of lateral flows

The effects of the lateral flow rates on the capsule dimensions and profiles are shown in Fig. 3.11. For a given fixed flow rate Ca = 0.05, $\lambda = 1$, $a/\ell_z = 0.9$, increasing lateral flow rates (thus stronger hydrodynamic forces) causes a significant change in the capsule's overall shape,i.e., capsule's length L_x increases significantly while its height L_z decreases. As seen in capsule profiles presented in Fig. 3.11 (d), capsules develop a pointed rear tail as lateral flow rates increase just after the capsule exits the cross-junction (i.e., at $x_c/\ell_z = 2$). In this case, the stronger hydrodynamic forces owning to increasing vertical flows also overcome the weak membrane tensions and thus the capsule needs to increase the tail curvature significantly to produce strong enough local interfacial forces. Furthermore, the capsule velocity is increased as depicted in Fig.3.11(c) since the average fluid velocity in the horizontal square channel after the cross-junction is increased.

3.4 Effects of viscosity ratio

In this section, we present our findings regarding the effects of viscosity ratio λ on the transient dynamics of a capsule in Figure 3.13. We investigate capsules with

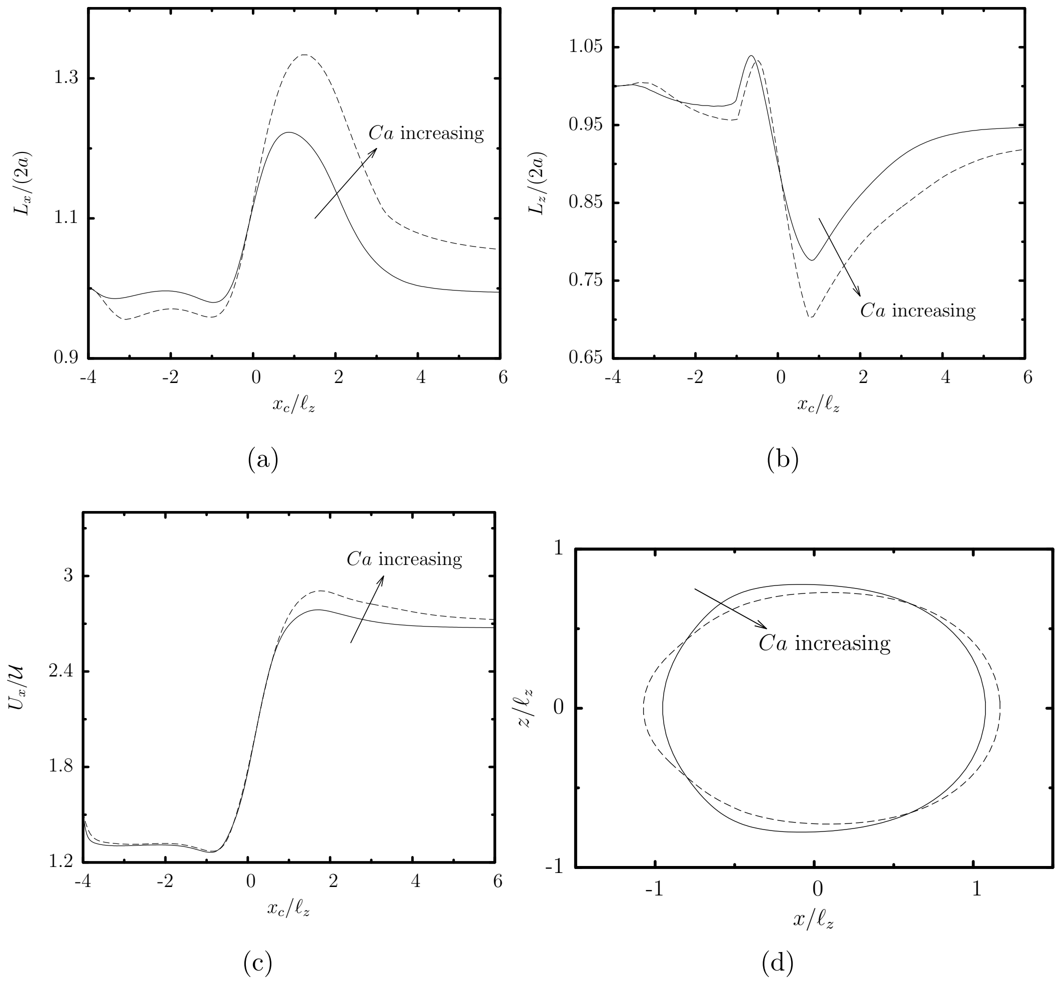

Figure 3.10: Evolution of capsule properties as a function of the centroid x_c, for a capsule with $a/\ell_z = 0.9$, $\lambda = 1$, $Q_v/Q = 0.5$ and capillary number $\mathrm{Ca} = 0.05, 0.1$. (a) Length L_x, and (b) height L_z of the capsule (scaled with the length $2a$ of the undisturbed spherical shape). (c) Capsule velocity U_x (scaled with the average undisturbed velocity $\mathcal{U}$ of the upstream horizontal channel). (d) Capsule profile (i.e., capsule intersection with the plane y=0) just after the cross-junction at $x_c/\ell_z = 2.13$ for $\mathrm{Ca} = 0.05, 0.1$.

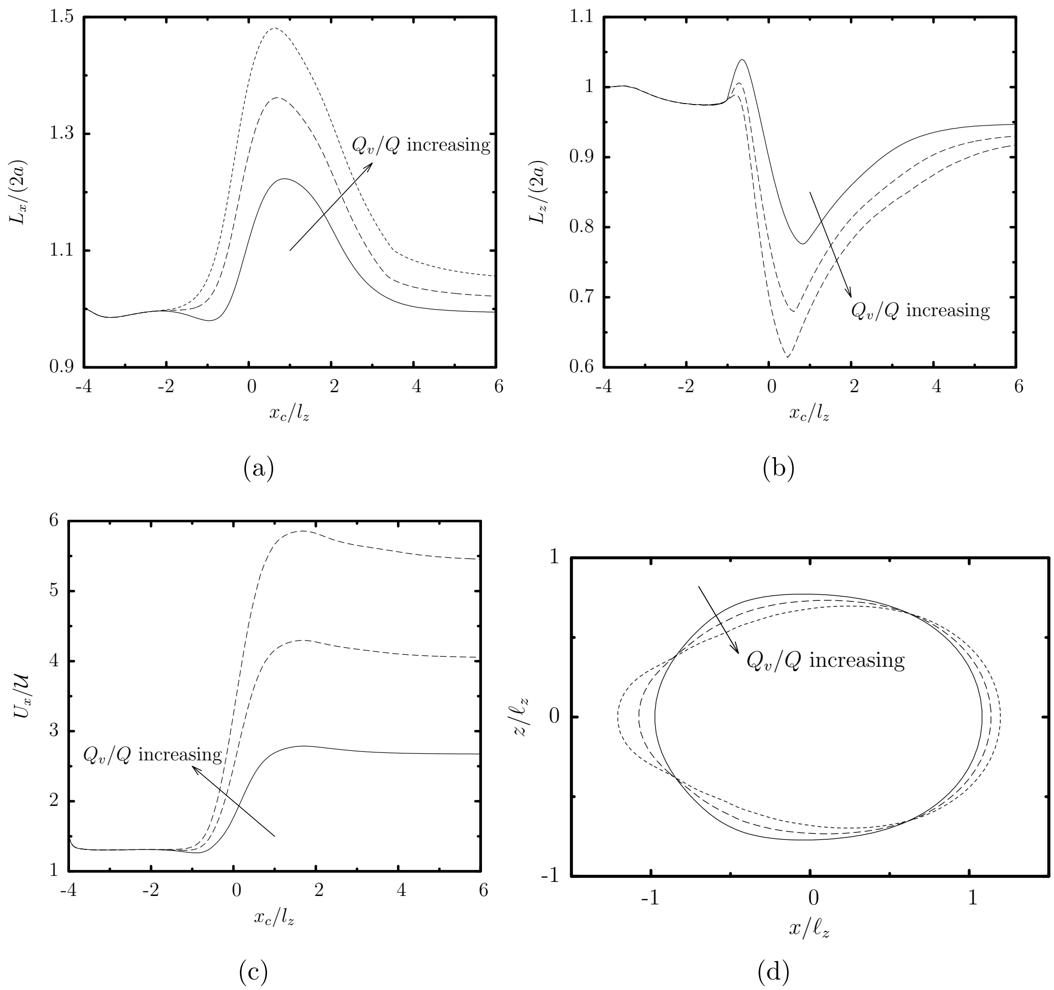

Figure 3.11: Evolution of capsule properties as a function of the centroid x_c, for a capsule with $a/\ell_z = 0.9$, $\lambda = 1$, Ca $= 0.05$ and lateral flows $Q_v/Q = 0.5, 1.0, 1.5$. (a) Length L_x, and (b) height L_z of the capsule (scaled with the length $2a$ of the undisturbed spherical shape). (c) Capsule velocity U_x (scaled with the average undisturbed velocity $\mathcal{U}$ of the upstream horizontal channel). (d) Capsule profile (i.e., capsule intersection with the plane y=0) just after the cross-junction at $x_v/\ell_z = 2$ for $Q_v/Q = 0.5, 1.0, 1.5$.

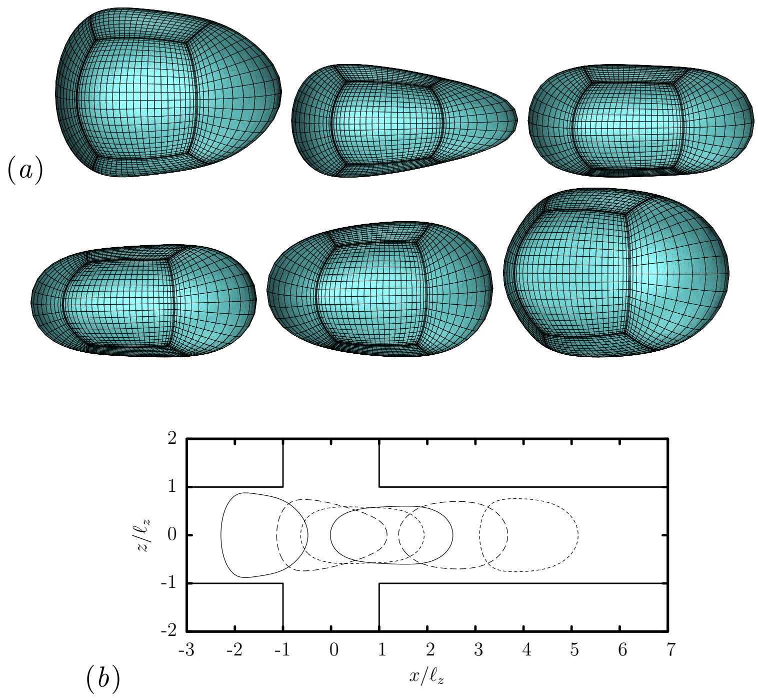

Figure 3.12: The shape of a capsule (plotted row-wise) with $a/\ell_z = 0.9$, Ca $= 0.05$, $\lambda = 5$, $Q_v/Q = 1.5$ inside the microfluidic device as seen from (a) the negative y-axis (i.e., front view) at centroid $x_c/\ell_z = -1.50, -0.07, 0.85, 1.42, 2.58, 4.18$. (b) As in (a) but for capsule profile (i.e., capsule intersection with the plane y=0).

$a/\ell_z = 0.9$, $Q_v/Q = 0.5$, and capillary number Ca $= 0.1$, while we vary the viscosity ratio in the range $\lambda = 0.01 - 5$, i.e., we investigate from inviscid to very viscous capsules. By comparing the capsule shapes shown in Figure 3.7 and Figure 3.2, we note that the overall capsule transient deformation is similar for viscosity ratios $\lambda = 0.01$ and $\lambda = 1$. The increase of its length L_x along with the corresponding decrease of its height L_z as shown in Figure 3.13 (a) and (b) result in the different shape transitions from elongated bullet-like to highly non-axisymmetric three-dimensional shapes. At $x_c/\ell_z = 1.42$, both low-viscosity and equiviscous capsules obtain an inverse bullet-like shapes owning to stronger hydrodynamic stresses. However, at $x_c/\ell_z = 2$ as seen in the capsule profile (i.e., capsule intersection with the plane $y = 0$) shown in Figure 3.13 (d), the rear development is different for low-viscosity and equiviscous capsules. The low-viscosity develops a pointed rear tail for interfacial stability reasons, while equiviscous capsules develop elongated and rounded edges. The transient deformation of high-viscosity (i.e., $\lambda = 5$) capsule is very different as shown in Figure 3.12 and is reduced inside the cross-junction due to the much slower deformation rate. These viscous capsules have an axisymmetric shape as they move through the cross-junction. It is of interest to note that the increased inner fluid viscosity prevents the development of a point rear edge. However, as the capsule exits the cross-junction and adopts the bullet-like shape in the square channel far downstream from the cross-junction (i.e., $x_c/\ell_z = 4.18$, the steady-state capsule deformation increases with the viscosity ratio λ as seen 3.13 (a) and (b). Note at $x_c/\ell_z = 2$, it is the very viscous capsules which are still affected by the cross-junction and have a fully three-dimensional shape since capsules with smaller viscosity ratio relax faster. It is of interest to observe that the capsule velocity U_x is practically not affected by λ as shown in Figure 3.13 (c) because of the weak inner fluid circulation, and thus all capsules show the same increase in U_x as they pass through the cross-junction.

To explain the effects of viscosity ratio on the transient deformation of capsule, note that the transient deformation results from a complex interaction between the hydrodynamic forces that deform the membrane and the elastic membrane tensions that resist the deformation. The capsule responds to the imposed flow change with an intrinsic response time that depends on the physical properties of the capsule (i.e., membrane hardness C) [25]. The capsule transient deformation is then characterized by the membrane time scale necessary to reach steady-state shape, which for a given

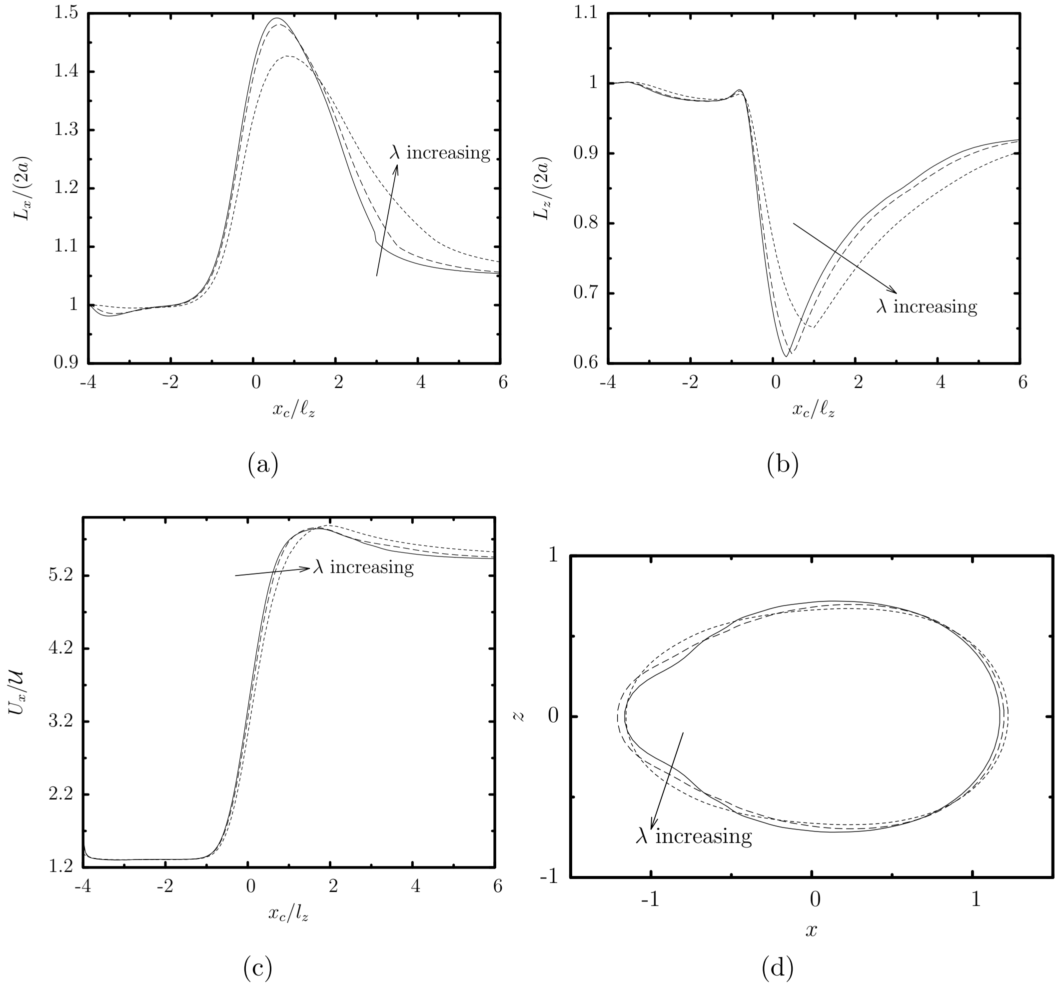

Figure 3.13: Capsule properties as a function of the centroid x_c, for a capsule with $a/\ell_z = 0.9$, $Q_v/Q = 1.5$, $\mathrm{Ca} = 0.05$ and viscosity ratio $\lambda = 0.01, 1, 5$. (a) Length L_x, and (b) height L_z of the capsule (scaled with the length $2a$ of the undisturbed spherical shape). (c) Capsule velocity U_x (scaled with the average undisturbed velocity $\mathcal{U}$ of the upstream horizontal channel). (d) Capsule profile (i.e., capsule intersection with the plane y=0) just after the cross-junction at $x_c/\ell_z = 2$ for $\lambda = 0.01, 1, 5$.

membrane hardness C is given by

$$\tau_m \sim (1+\lambda)\mathrm{Ca}\frac{a}{\ell_z}\tau_f \tag{3.7}$$

where $\tau_f = \ell_z/\mathcal{U}$ is the flow time scale. Note that this membrane response time has been studied for capsules in transient elongational flows [18] and for transient dynamics of an elastic capsule in a microfluidic constriction [25]. Using Eqn. 3.7 for the low-viscosity capsules,e.g. for $\lambda = 0.01$, the membrane time scale τ_m does not vary with λ but is influenced by the flow rate Ca. Therefore, the inner fluid of the capsule does not have a significant effect on the capsule transient deformation. Therefore, as illustrated in Figure 3.13 (d) for various viscosity ratios, it is the low-viscosity capsule that has developed a pointed rear tail at $x_c/\ell_z = 2$ for interfacial stability reasons. The membrane time scale τ_m necessary for the low-viscosity capsule to react to the flow changes imposed by the cross-junction is decreased; therefore, making the deformation rate faster. However, during the final relaxation stage towards the steady-state shape at $x_c/\ell_z = 4.18$, the capsule membrane time response (i.e., τ_m) is fast enough for the low-viscosity capsule to adapt and be in dynamic equilibrium with the external flow. As the viscosity ratio increases to $\lambda = 1$, both the inner and the surrounding fluids affect the capsule transient deformation. The membrane time scale τ_m necessary for the capsule to adapt to the flow changes imposed by the cross-junction is increased only moderately with λ. Therefore, the deformation rate is moderately slower as the equiviscous capsule passes the cross-junction at $x_c/\ell_z = 2$. Far from the cross-junction at $x_c/\ell_z = 4.18$, the equiviscous capsule obtains a dynamic equilibrium bullet-like shape. For the very viscous capsules (e.g. $\lambda = 5$), it is the inner fluid which mostly affects the capsule deformation. For such capsule, the membrane time scale τ_m necessary for the capsule to react to the flow change imposed by the cross-junction is increased considerably, being proportional to λ as seen in Eqn. 3.7. This makes the deformation rate much slower as these capsules pass through the cross-junction. The capsule transient deformation is decreased due to the increased membrane time scale τ_m. However, during the final relaxation stage far downstream from the cross-junction at $x_c/\ell_z = 4.18$, the very viscous capsules are still affected by the increased hydrodynamic forces from the incoming flows of the cross-junction and have a deformed axisymmetric shape. These capsules need a significant time (or channel length) to obtain the steady-state parachute-like shape in agreement with Eqn.3.7 and our computational findings shown in Figure 3.12.

3.5 Conclusion

In this chapter, we investigate computationally the transient dynamics of an elastic capsule flowing along the centerline of a cross-junction microchannel. In particular, we consider an initially spherical capsule with a size smaller than the cross-section of the square channels comprising the cross-junction, and investigate the effects of the capsule size, flow rate, lateral flow rates, and fluid viscosity ratio on the transient capsule dynamics and deformation. Our investigation shows that the intersecting flows at the cross-junction act like a constriction, created by the streamlines of the intersecting flows, and thus the capsule needs to be compressed inside and outside of this constriction. Therefore, the capsule shows a rich deformation behavior as it passes through the micro-junction. After obtaining a bullet-like shape in the square channel before the cross-junction, the capsule becomes slender inside the junction (to accommodate the intersecting flows), then it obtains an inverse-bullet shape as it exits the cross-junction which reverts to a more deformed bullet-like shape far downstream of the cross-junction (owing to the combined flow rates of the intersecting channels). As the capsule size increases, its deformation increases and larger capsules owning to higher flow blocking take more time to pass through the cross-junction. As the viscosity ratio decreases, the capsule's transient deformation increases and a tail formation develops transiently, especially for the low-viscosity capsule. However, the viscosity ratio does not affect much the capsule velocity due to a weak inner fluid circulation. Our findings suggest that the tail formation of low-viscosity capsule may promote membrane breaking and thus drug release of pharmaceutical capsules in the microcirculation. For example, if one needs to fabricate artificial capsules for drug delivery, the use of low-viscosity capsules is relevant and knowing the weak points of the membrane as shown in figure 3.2 where a pointed tail(thus mechanical instability) is developed, capsules with higher viscosity ratio can be fabricate to prevent rupture in the cross-junction during capsule fabrication.

Chapter 4: Motion of an elastic capsule in a microfluidic T-junction

4.1 Problem description

In this section, we consider a three-dimensional capsule enclosed by an elastic membrane flowing inside a microfluidic T-junction as illustrated in Figure 4.1. The T-junction is constructed from one square horizontal microfluidic channel intersecting with a vertical square microfluidic channel without crossing it but forming a T-shape with cross-section half lengths $\ell_y = \ell_z$. The origin of the co-ordinate system is placed at the center of the junction. We think of one channel as horizontal and the other as vertical as illustrated in Figure 4.1. At time $t = 0$, the capsule is located upstream of the T-junction in the horizontal channel having a spherical shape with radius a and centroid x_c = -4ℓ_z. That instant, the flow is turned on inside of the microfluidic device and we investigate the motion of the capsule as it enters and exits the microfluidic T-junction which occupies the x-region [-ℓ_z,ℓ_z].

The capsule's interior and exterior fluids are Newtonian fluids, with viscosities $\lambda\mu$ and μ, and have equal density (i.e., no buoyancy and sedimentation effects). We define the capsule size by $a = (3V/4\pi)^{1/3}$ where V is the capsule volume. It is

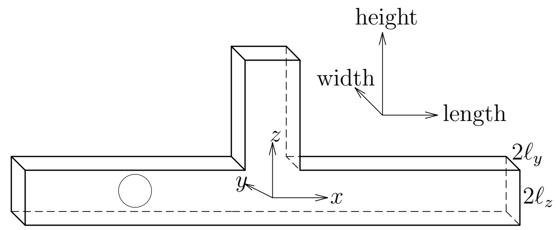

Figure 4.1: Illustration of an elastic capsule flowing at the centerline of a microfluidic T-junction.

important to assume that the capsule has a negligible membrane permeability(i.e., no flow through the membrane) and its volume is constant. At the inlet upstream of the T-junction in the horizontal channel, a velocity flow profile is imposed as well as no-slip and no penetration boundary conditions are imposed on solid walls. Far from the capsule, the flow approaches the undisturbed flow $\boldsymbol{u}^{\infty}$ in a channel characterized by a constant flow rate $Q = 4\mathcal{U}\ell_z^2$.

$$\frac{u_x^{\infty}}{\Upsilon} = (\ell_z^2 - z^2) + \sum_{m=1}^{\infty} B_m \cosh\left(\frac{b_m y}{\ell_z}\right) \cos\left(\frac{b_m z}{\ell_z}\right) \tag{4.1}$$

where

$$\Upsilon = -\frac{1}{2\mu}\frac{dp}{dx}, \quad b_m = \frac{(2m-1)\pi}{2}, \qquad B_m = \frac{(-1)^m 4\ell_z^2}{b_m^3 \cosh\left(\frac{b_m \ell_y}{\ell_z}\right)}, \tag{4.2}$$

where p is the dynamic pressure. To compute the volumetric flow rate Q over the cross-section area, we integrate Eq. (3.1)

$$\frac{Q}{\Upsilon} = \frac{8\ell_y\ell_z^3}{3} + \sum_{m=1}^{\infty} B_m \left(\frac{2\ell_z}{b_m}\right)^2 \sinh\left(\frac{b_m \ell_y}{\ell_z}\right) \sin(b_m) \tag{4.3}$$

The average velocity of the exterior fluid far from the capsule is $\mathcal{U} = Q/(\ell_z^2)$ The capsule velocity in the flow direction U_x may be different than the average velocity $\mathcal{U}$ in the horizontal channel. The incoming flow rate at each of the two inlets of the vertical microchannel is defined as Q_v. After the T-junction, the horizontal channel has a total constant flow rate of $(Q + Q_v)$. We assume that the Reynolds-number is small for both the surrounding and inner flows, thus the capsule motion occurs in the Stokes regime.

Furthermore, we consider a slightly over-inflated capsule made from a thin strain-hardening elastic membrane obeying the Skalak *etal.* constitutive law [52] with comparable shearing and area-dilatation resistance. Due to osmotic effects and a positive osmotic pressure difference p^0 between the capsule's interior and exterior fluids [17], the capsule membrane in this work is prestressed (over-inflated) by an isotropic elastic tension to account for the osmotic effects [6] and prevent buckling instabilities [28]. To add the capsule over-inflation, we define the prestress parameter α_p such that all lengths in the undeformed capsule would be scaled by $(1 + \alpha_p)$, relative to the reference shape [25]. Since the capsule is initially spherical, its membrane is initially prestressed by an isotropic elastic tension $\tau_0 = \tau_\beta^P(t = 0)$ which depends on the employed constitutive law and its parameters but not on the capsule size. For example, given a Skalak capsule with membrane hardness $C = 1$ and prestress $\alpha_p = 0.05$ considered in this problem, the undisturbed capsule size is 5 % higher than that of the reference shape and the initial membrane tension due to prestress is $\tau/G_s \approx 0.3401$. The capsule motion depends on four additional dimensionless parameters: the capsule size (relative to the channel height) a/ℓ_z, the relative lateral flow rate Q_v/Q, the viscosity ratio λ, and the capillary number Ca defined as

$$\mathrm{Ca} = \frac{\mu \mathcal{U}}{G_s} \tag{4.4}$$

where $\mathcal{U}$ is the average flow velocity in the upstream horizontal channel before the T-junction.

We investigate the motion of elastic capsule with varying initial lateral position (z_c^0/ℓ_z), size (a/ℓ_z), flow rate (Ca) and lateral flow rates (Q_v/Q). Note that the capillary number, as defined by Eq. 4.4, does not contain any length scale and thus it may be considered as a dimensionless flow rate. In this study, the channel's half-height ℓ_z is used as the length scale, the velocity is scaled with the average undisturbed velocity $\mathcal{U}$ of the upstream horizontal channel, and thus the time scale is $\tau_f = \ell_z/\mathcal{U}$.

4.2 Results and Discussion

Figure 4.2 shows results of simulations of capsule with $a/\ell_z = 0.5$, $\lambda = 1$, $\mathrm{Ca} = 0.1$, and $Q_v/Q = 0.5$ inside the T-junction microchannel. Capsule shapes are shown from the negative y-axis (i.e., front view) at centroid $x_c/\ell_z = -1.0, 0.0, 0.5, 1.4$. At initial instant, the capsule is placed at the initial lateral position, $z_c^0/\ell_z = 0.3$ near the top channel's wall and moves laterally away from the wall and much more downward at the intersecting flows. Inside the T-junction, the capsule aligns itself along the flow direction and attains an ellipsoidal shape. After the T-junction, the capsule still has the ellipsoidal shape and moves along the centerline of the T-junction microchannel.

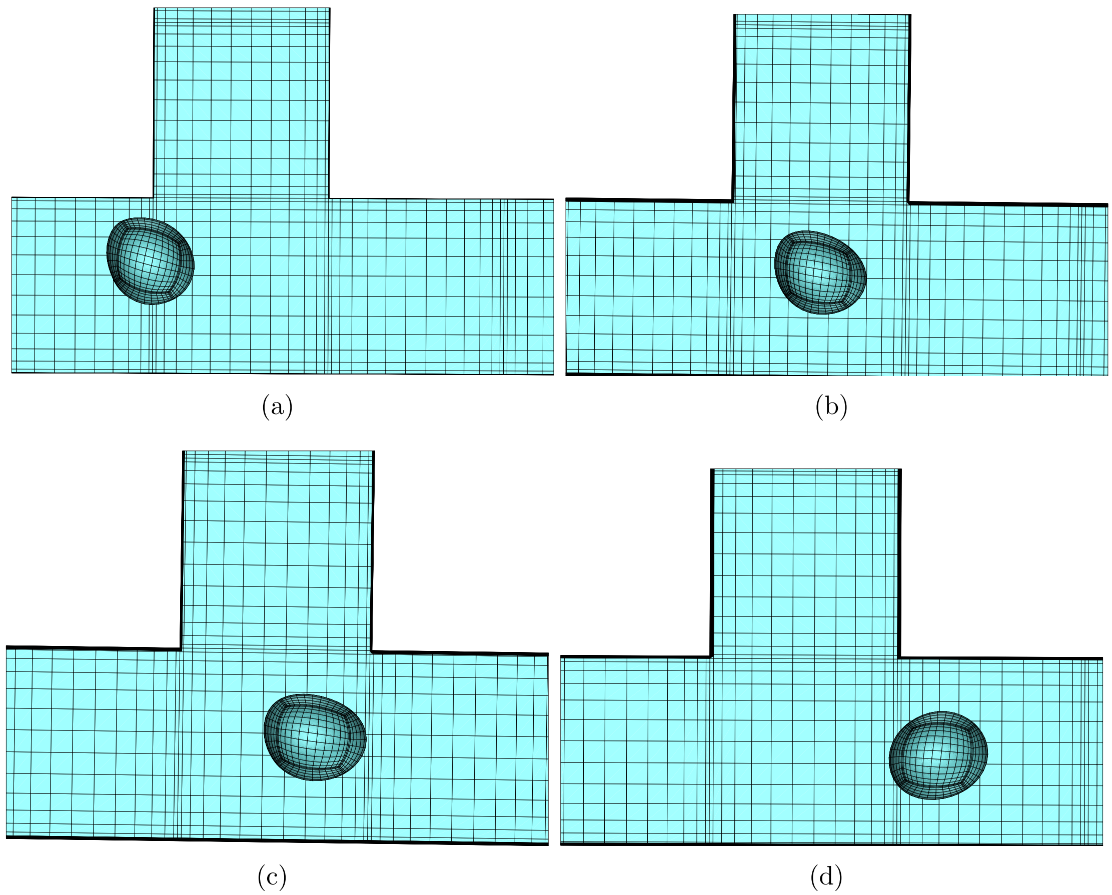

Figure 4.2: The shape of a capsule (plotted row-wise) with $a/\ell_z = 0.5$, $\lambda = 1$, $\mathrm{Ca} = 0.1$, $Q_v/Q = 0.5$, initial lateral position,$z_c^0/\ell_z = 0.3$ inside the microfluidic device as seen from the negative y-axis (i.e., front view) at centroid x_c/ℓ_z (a)-1.0, (b) 0.0, (c) 0.5, (d)1.4.

4.2.1 Effects of initial lateral position

We now study the effects of capsule initial lateral position on the motion of capsule inside the microfluidic T-junction device. In particular, we consider the capsule with $a/\ell_z = 0.5$, $Ca = 0.1$, $\lambda = 1$, $Q_v/Q = 0.5$ and investigate the transient motion for various initial lateral position i.e., $z_i^0/\ell_z = 0.3, 0.5, 0.6$. Figure 4.3 (a) reveals that the capsule initial lateral position does not affect the capsule deformation as the capsule enters the T-junction. However, as the caspule exits the T-junction, the capsule deformation decreases as the initial lateral position increases. The capsule below the centerline (i.e., $z_c^0/\ell_z = -0$) is still affected by the T-junction. The capsule at the centerline of the microchannel shows a sudden increase and decrease in L_x at $x_c/\ell_z = 3$. Figure 4.3 (b) and (c) shows that as the initial lateral position increases, the capsule moves faster and reaches different final lateral positions as it moves toward the centerline. Note that Figure 4.3 (d) shows that as the capsule enters the T-junction, the capsule migration velocity U_z decreases until it reaches a minimum at $x_c/\ell_z = 0$. The minimum value of the capsule migration velocity U_z increases as the initial lateral position increases. As the capsule exits the T-junction, it migrates away from the microchannel's wall towards the centerline at different lateral migration velocities U_z.

4.2.2 Effects of capsule size

In the present section, we study the effects of the capsule size on the capsule motion inside the microfluidic T-junction device. In particular, we consider cap-

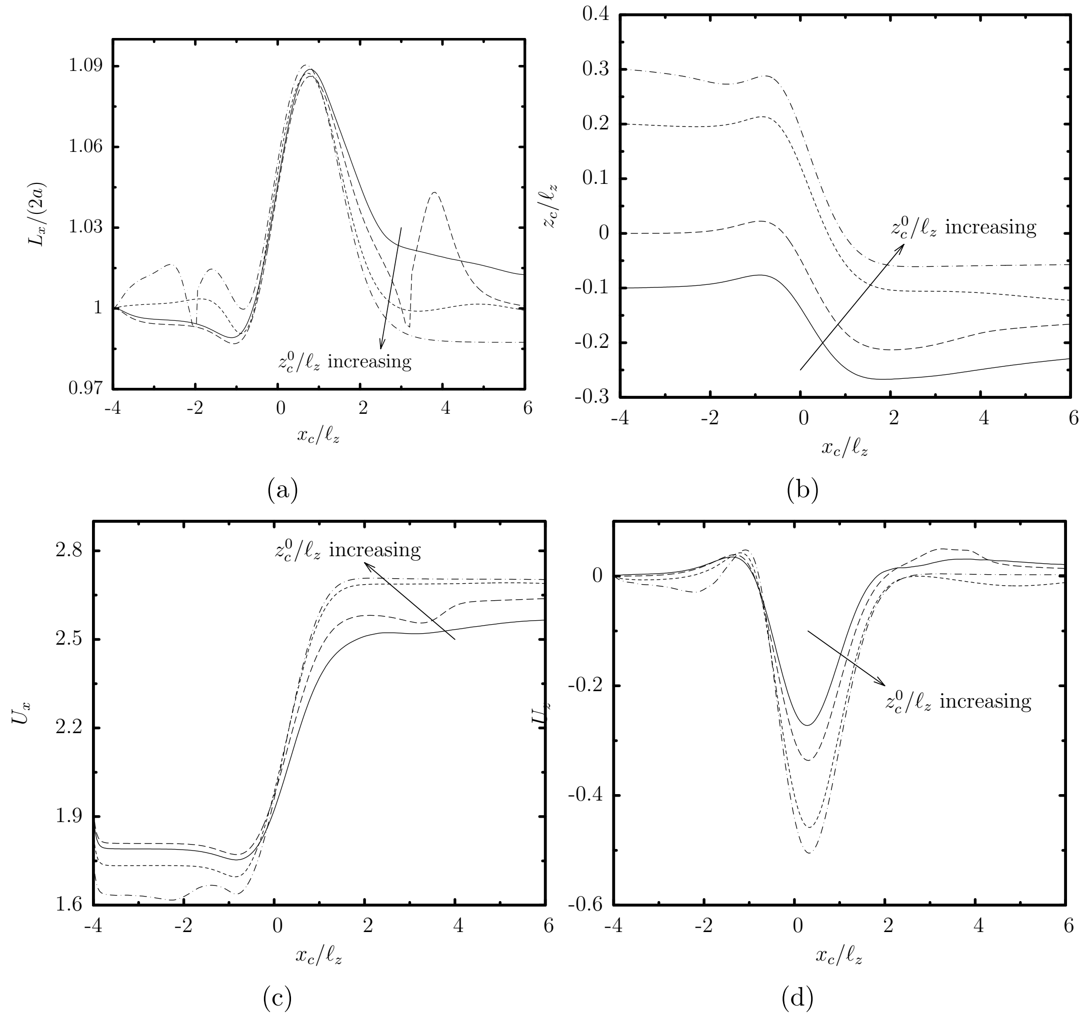

Figure 4.3: Evolution of capsule properties as a function of the centroid x_c, for a capsule with Ca $= 0.05$, $\lambda = 1$, $Q_v/Q = 0.5$, and varying initial lateral position, $z_c^0/\ell_z = -0.1, 0.0, 0.2, 0.3$. (a) Length L_x, and (b) lateral position z_c of the capsule (scaled with the cross-section half-length ℓ_z). (c) Capsule velocity U_x (scaled with the average undisturbed velocity $\mathcal{U}$ of the upstream horizontal channel). (d) Capsule lateral velocity U_z (scaled with the average undisturbed velocity $\mathcal{U}$ of the upstream horizontal channel.

sules with $Ca = 0.05$, $z_c^0/\ell_z = 0.2$, $\lambda = 1$, $Q_v/Q = 0.5$ and investigate the transient motion for various capsule sizes i.e., $a/\ell_z = 0.1, 0.2, 0.3, 0.5, 0.6$. Figure 4.4 reveals that as the capsule size increases (thus higher flow blocking), the stronger hydrodynamic forces cause the capsule to extend along the flow direction, i.e., the capsule's length L_x increases as the capsule enters the T-junction, reaches a peak inside the T-junction and decreases as the capsule exits the T-junction. There is a small lateral migration towards the microchannel centerline as shown in Figure 4.4 (b) as the capsule size increases. After the T-junction, larger capsules tend to migrate away from the lower wall toward the centerline of the T-junction of microchannel. This migration away from the wall due the stronger lateral lift repulsion forces exerted on the capsule is in agreement with Goldsmith glass tube observations [36]. Experimental and numerical studies on non inertial lateral migration of vesicles in bounded Poiseuille flow by Coupier *et al.* [13] showed that the combined effects of the walls and of the curvature of the velocity profile induce a lateral migration toward the centerline of the channel. Vesicles close to the wall wall experience stronger lateral repulsion forces which push them away from the wall because of the lubrication pressure from the gap between vesicles and the wall of the channel. These lateral repulsion forces decrease as the distance between the vesicles and the wall of the channel increases (or as the vesicle size decreases) and become zero when the capsule reaches to the centerline. These observations are in agreement with our results. As the capsule enters the T-junction, its velocity U_x increases until it reaches a maximum and remains constant at maximum as the capsule exits the T-junction. However, this velocity decreases as the capsule size increases due to the higher flow blocking. On the other hand, the capsule migration velocity U_z decreases as the capsule enters the T-junction and reaches a peak inside the T-junction. It starts to increase as the capsule migrates away from the microchannel's wall toward the centerline. As the capsule approaches the low-shear region near the centerline, its migration velocity declines to zero. Note that the capsule migration velocity U_z is less affected by the capsule size for the capsule size considered in this problem. However, larger capsules are shown to migrate slightly faster away from the wall toward the microchannel centerline because they experience stronger lateral repulsion forces as the distance between the capsules and wall of the channel decreases.

4.2.3 Effects of flow rate

In the present section, we study the effects of the flow rate on the capsule motion inside the microfluidic T-junction device. In particular, we consider capsules with $a/\ell_z = 0.5$, $z_c^0/\ell_z = 0.2$, $\lambda = 1$, $Q_v/Q = 0.5$ and investigate the transient motion for various capillary numbers i.e., $\mathrm{Ca} = 0.02, 0.05, 0.1$. Figure 4.5 shows the evolution of the capsule properties as a function of the centroid x_c. As Ca increases, the stronger hydrodynamic forces cause the capsule to extend along the flow direction (i.e., the capsule's length L_x increases as the capsule enters the T-junction). As the capsule exits the T-junction, its L_x decreases as shown in Figure 4.5 (a). Figure 4.5 (b) reveals that there is a small lateral migration away from the microchannel centerline as Ca increases. Both the capsule velocity U_x and migration velocity U_z are not affected by the flow rate Ca as shown in Figure 4.5

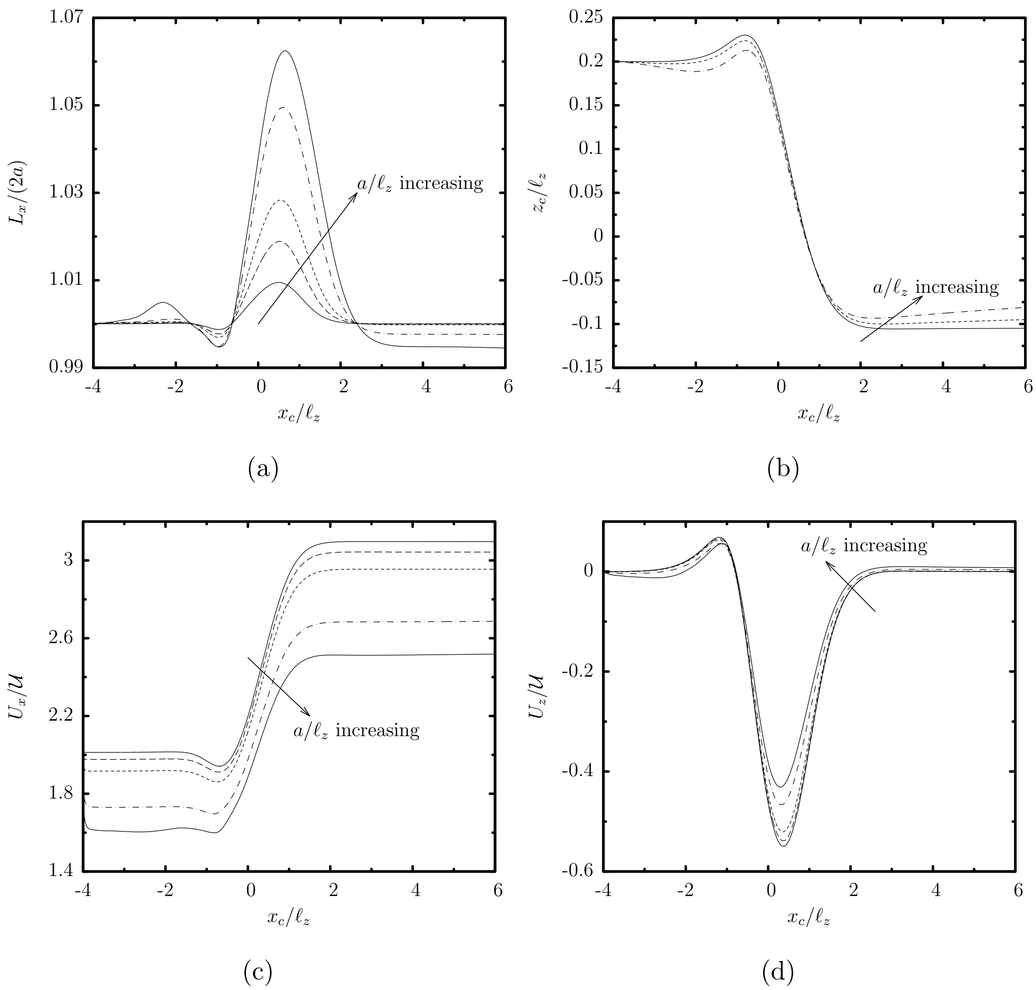

Figure 4.4: Evolution of capsule properties as a function of the centroid x_c, for a capsule with Ca $= 0.05$, $\lambda = 1$, $Q_v/Q = 0.5$, $z_c^0/\ell_z = 0.2$ and varying size $a/\ell_z = 0.1, 0.2, 0.3, 0.5, 0.6$. ($a$) Length L_x, and (b) lateral position z_c/ℓ_z of the capsule (scaled with the cross-section half-length ℓ_z). (c) Capsule velocity U_x (scaled with the average undisturbed velocity $\mathcal{U}$ of the upstream horizontal channel). (d) Capsule lateral velocity U_z (scaled with the average undisturbed velocity $\mathcal{U}$ of the upstream horizontal channel.

(c). However, far away from the T-junction, the capsule migration velocity decreases as Ca increases.

4.2.4 Effects of viscosity ratio

The effects of viscosity ratio on the evolution of capsule properties are shown in Figure 4.6. For a given fixed Ca $= 0.05$, $a/\ell_z = 0.5$, $z_c^0/\ell_z = 0.3$, and $Q_v/Q = 0.5$, increasing the viscosity ratio (*i.e.*, $\lambda = 0.01, 0.1, 1, 5, 10$) causes a significant change in the capsule's overall shape (i.e., capsule's length L_x decreases significantly as the capsule enters and exits the T-junction). After the T-junction (i.e., $x_c/\ell_z = 2$), it is the very viscous capsule that is still affected by the T-junction and is still deformed since capsules with smaller viscosity ratio relax faster. The present prediction is in agreement with the effects of viscosity ratio on the capsule dynamics in a cross-junction microchannel discussed in details in Section 3.4. The capsule lateral position z_c/ℓ_z, velocity U_x and migration velocity U_z are practically not affected by the viscosity ratio λ as shown in Figure 4.6 (c). Because of the weak inner fluid circulation, and thus all capsules show the same increase in U_x and U_z as they pass through the T-junction.

4.2.5 Effects of lateral flow rate

The effects of lateral flow rate on the motion of capsule flowing inside the T-junction microchannel are illustrated in Figure 4.7. In particular, we consider capsules with $Ca = 0.05$, $z_c^0/\ell_z = 0.3$, $\lambda = 1$, and investigate the transient motion for

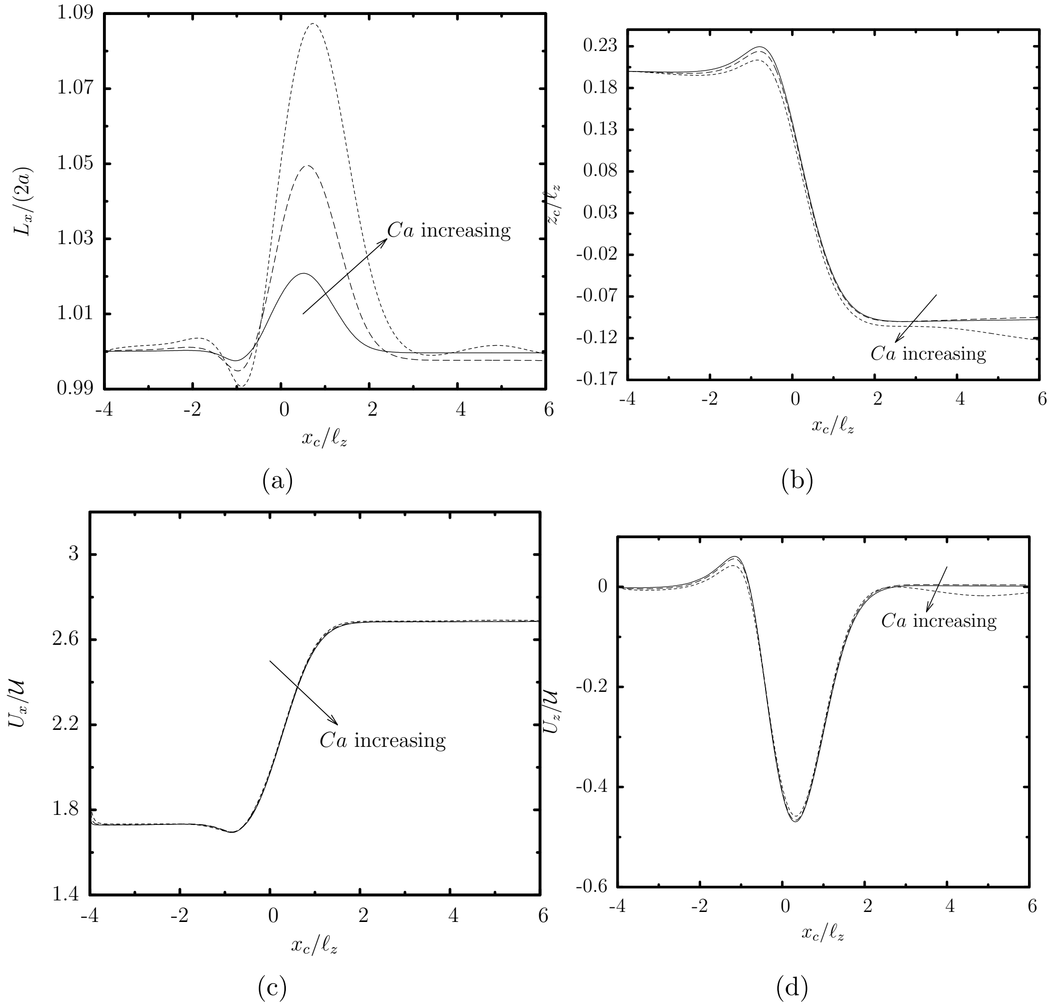

Figure 4.5: Evolution of capsule properties as a function of the centroid x_c, for a capsule with $a/\ell_z = 0.5$, $\lambda = 1$, $Q_v/Q = 0.5$, $z_c^0/\ell_z = 0.2$ and varying capillary number $\mathrm{Ca} = 0.02, 0.05, 0.1$. (a) Length L_x, and (b) lateral position z_c/ℓ_z of the capsule (scaled with the cross-section half-length ℓ_z). (c) Capsule velocity U_x (scaled with the average undisturbed velocity $\mathcal{U}$ of the upstream horizontal channel). (d) Capsule lateral velocity U_z (scaled with the average undisturbed velocity $\mathcal{U}$ of the upstream horizontal channel.

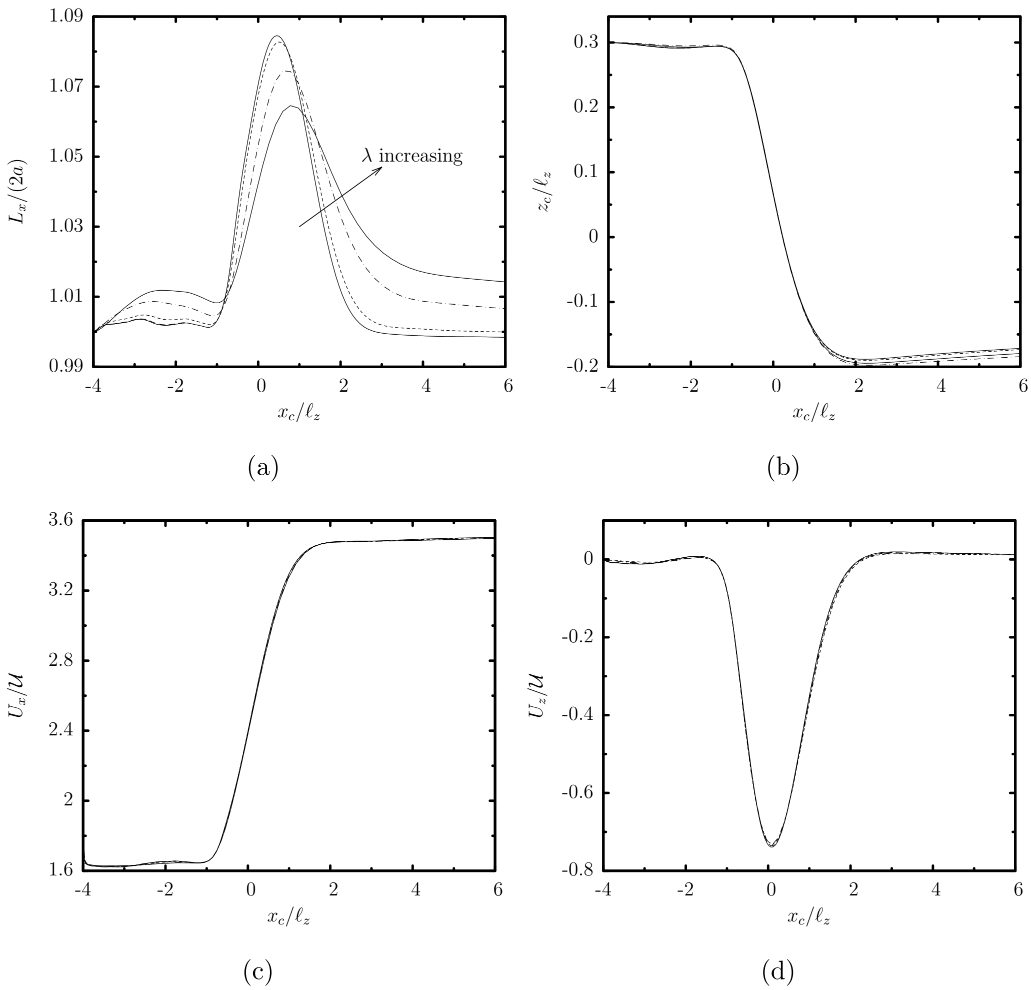

Figure 4.6: Evolution of capsule properties as a function of the centroid x_c, for a capsule with Ca $= 0.05$, $a/\ell_z = 0.5$, $Q_v/Q = 0.5$, $z_c^0/\ell_z = 0.3$, and viscosity ratio $\lambda = 0.01, 0.1, 1, 5, 10$. (a) Length L_x, and (b) lateral position z_c/ℓ_z of the capsule (scaled with the cross-section half-length ℓ_z). (c) Capsule velocity U_x (scaled with the average undisturbed velocity $\mathcal{U}$ of the upstream horizontal channel). (d) Capsule lateral velocity U_z (scaled with the average undisturbed velocity $\mathcal{U}$ of the upstream horizontal channel.

varying lateral flow rate i.e., $Q_v/Q = 0.5, 0.75, 1$. Results reveal that as the lateral flow rate increases, the stronger hydrodynamic forces cause the capsule to extend along the flow direction, i.e., the capsule's length L_x increases inside the T-junction. As the channel's lateral flow rate increases, the capsule lateral displacement z_c moves laterally much more downward at the intersecting flows and remains almost constant. As the capsule enters the T-junction, its velocity U_x increases due to the increasing lateral flows until it reaches a peak inside the T-junction and remains constant at the peak far downstream of the T-junction. On the other hand, as the lateral flow rate increases the capsule migration velocity U_z decreases until it reaches a minimum at $x_c/\ell_z = 0$. However, as the capsule exits the T-junction, it migrates away from the microchannel's wall toward the centerline at the same migration velocity U_z until U_z declines to zero near the centerline.

4.3 Conclusion

We investigate via numerical computations the motion of an elastic capsule (made from elastic membranes obeying the strain-hardening Skalak law) flowing inside the microfluidic T-junction device. We consider capsules with size smaller than the cross-section of the square channels comprising the T-junction, and investigate the effects of the capsule initial lateral position, capsule size, flow rate, lateral flow rate, and fluid viscosity ratio on the motion of these capsules in the T-junction michrochannel. As the capsule initial lateral position increases, the capsule moves faster and reaches different final lateral positions. As the capsule size increases,

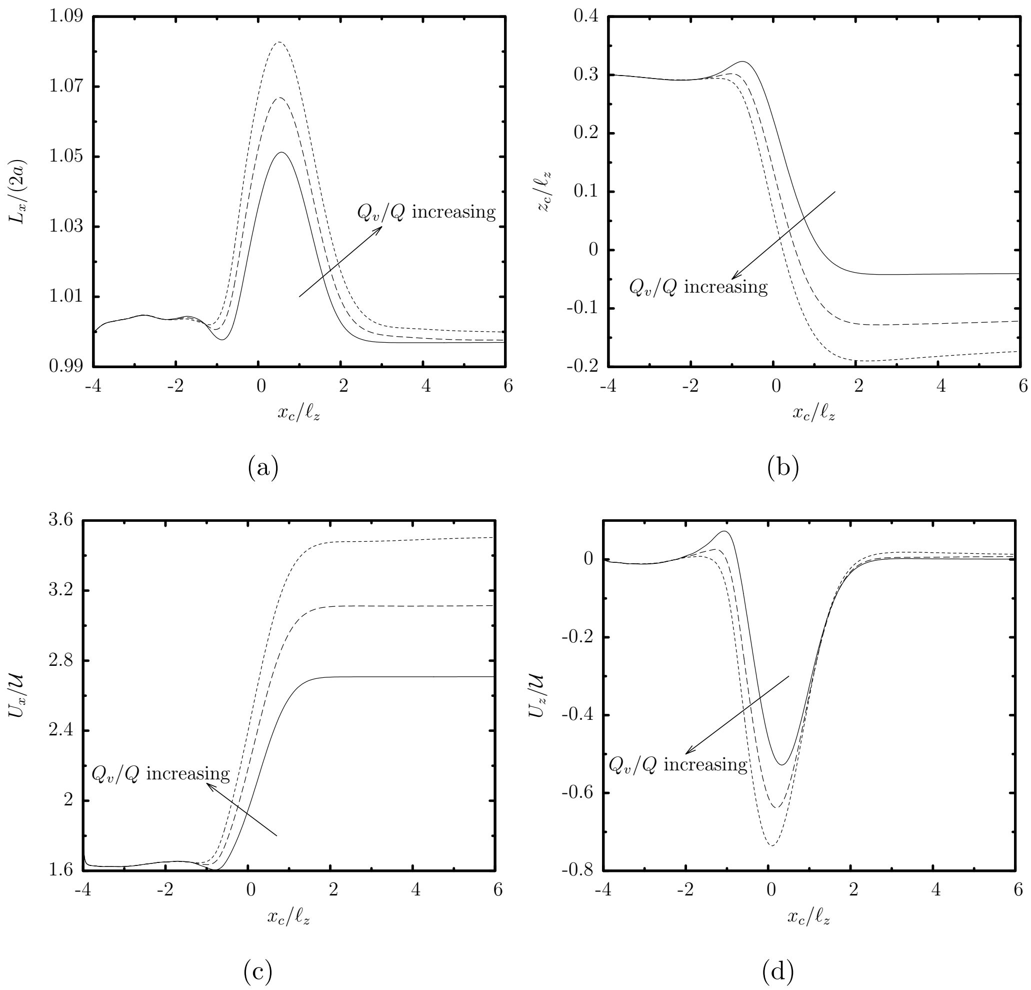

Figure 4.7: Evolution of capsule properties as a function of the centroid x_c, for a capsule with $\mathrm{Ca} = 0.05$, $a/\ell_z = 0.5$, $\lambda = 1$, $z_c^0/\ell_z = 0.3$ and lateral flow rate $Q_v/Q = 0.5, 0.75, 1$. (*a*) Length L_x, and (*b*) lateral position z_c/ℓ_z of the capsule (scaled with the cross-section half-length ℓ_z). (*c*) Capsule velocity U_x (scaled with the average undisturbed velocity $\mathcal{U}$ of the upstream horizontal channel). (*d*) Capsule lateral velocity U_z (scaled with the average undisturbed velocity $\mathcal{U}$ of the upstream horizontal channel.

the gap between the capsule surface and the channel wall decreases and this results in development of stronger hydrodynamic forces and a decrease in the capsule velocity due to the flow blocking. There is a small lateral migration towards the microchannel centerline as the capsule size increases. The capsule migrates towards the centerline, the low-shear region of the T-junction microchannel. This migration is in agreement with experimental and numerical studies on noninertial lateral migration of vesicles in bounded Poiseuille flow by Coupier *et al.* [13] which showed that the combined effects of the walls and of the curvature of the velocity profile induce a capsule migration toward the centerline of the channel. As Ca increases, the stronger hydrodynamic forces cause the capsule to extend along the flow direction (i.e., the capsule's length L_x increases as the capsule enters the T-junctions and L_x decreases as the capsule exits the T-junction). There is a small lateral migration away from the microchannel centerline as Ca increases. Both the capsule velocity U_x and migration velocity U_z are not affected by the flow rate Ca. The capsule lateral position z_c, velocity U_x and migration velocity U_z are practically not affected by the fluid viscosity ratio λ. As the channel's lateral flow rate increases, the capsule lateral displacement z_c/ℓ_z moves laterally much more downward at the intersecting flows. Our findings on the lateral migration in the T-junction microchannel suggest that there is a great potential for designing a T-junction microfluidic device that can be used to manipulate artificial and biological capsules. Geislinger *et al.* [35] designed a T-junction microchannel device to sort out red blood cells from blood plasma using non-inertial hydrodynamic lift at low Reynolds number. Furthermore, Geislinger *et al.* [34] developed a similar microfluidic device to sort out red blood cells from cancer cells.

Bibliography

[1] A. Ammala, Biodegradable polymers as encapsulation materials for cosmetics and personal care markets, *Int. J. Cosmet Sci* **35**, 113-24 (2013).

[2] P. Bagchi, Mesoscale simulation of blood flow in small vessels, *Biophysical Journal* **92** 1858 - 1877 (2007).

[3] D. Barthès-Biesel, Motion and Deformation of Elastic Capsules and Vesicles in Flow, *Annu. Rev.Fluid Mech.* **48**, 25-52 (2016).

[4] D. Barthès-Biesel, X.-Q. Hu,B.Sévénié, A.-V. Salsac, and E. Leclerc, Characterizing the membrane properties of capsules flowing in a square-section microfluidic channel: Effects of the membrane constitutive law, *Phys.Rev.E* **87**, 063008 (2013)

[5] D. Barthès-Biesel, X.-Q. Hu, and A.-V. Salsac, Flow of a spherical capsule in a pore with circular or square cross-section, *J. Fluid Mech.* **705**, 176-194 (2012).

[6] D. Barthès-Biesel, Modeling the motion of capsules in flow, *J. Colloid Interface Sci.* **16**, 3-12 (2011)

[7] D. Barthès-Biesel, E.Leclerc, Y. Lefebvre,J. Walter, F. Edwards-Levy, Flow of artificial microcapsules in microfluidic channels: a method for determining the elastic properties of the membrane, *Phys. Fluids* **20**, 123102 (2008).

[8] D. Barthès-Biesel and C. Quéguiner, Axisymmetric motion of capsules through cylindrical channels, *J. Fluid Mech.* **348**, 349-376 (1997).

[9] D. Barthès-Biesel and Y. Lefebvre, Motion of a capsule in a cylindrical tube: effect of membrane pre-stress, textitJ. Fluid Mech. **589**, 157-181 (2007).

[10] D. Barthès-Biesel , A. Diaz , and E. Dhenin, Effect of constitutive laws for two-dimensional membranes on flow-induced capsule deformation, *J. Fluid Mech.* **460**, 211-222 (2002)

[11] D. Barthès-Biesel and A. Diaz, Entrance of a bioartificial capsule in a pore, *Comput.Model. Eng. Sci.* **3**,321-337 (2002)

[12] D. Barthès-Biesel, Motion of a spherical microcapsule freely suspended in a linear shear flow. *J. Fluid Mech.* **100** , 853 (1980).

[13] G. Coupier, B. Kaoui, T. Podgorski and C. Misbah, Noninertial lateral migration of vesicles in bounded Poiseuille flow, *Phys. Fluids* **20**, 11702 (2008).

[14] I. T. Carvalho, B. N. Estevinho, and L. Santos, Application of microencapsulated essential oils in cosmetic and personal healthcare products - a review, *Int. J. Cosmet Sci* **38**, 109-119(2016)

[15] C. Champagne and P. Fustier, Microencapsulation for the improved delivery of bioactive compounds into foods, *Curr Opin Biotechnol* **18**, 184-90 (2007)

[16] G. Coupier, A. Farutin, C. Minetti, T. Podgorski and C. Misbah, Shape diagram of vesicles in Poiseuille flow, *Phys. Rev. Lett.* **108**, 178106 (2012).

[17] F. Risso, F. Colle-Pailot and M. Zagzoul, Experimental investigation of a bioartificial capsule flowing in a narrow tube, *J. Fluid Mech.* **547**, 149-173 (2006).

[18] A. Diaz, D. Barthès-Biesel, N. Pelekasis, Transient response of a capsule subjected to varying flow conditions: effect of internal fluid viscosity and membrane elasticity, *Phys. Fluids* **12**, 948-957 (2000)

[19] N. Boruah and P. Dimitrakopoulos, Motion and deformation of a droplet in a microfluidic cross-junction, *Soft Matter* **11**, 2782-2793 (2015)

[20] P. Dimitrakopoulos and S. Kuriakose, Determining a membrane's shear modulus, independent of its area-dilatation modulus, via capsule flow in a converging micro-capillary, *Soft Matter* **11**, 2782-2793 (2015).

[21] P. Dimitrakopoulos and Dodson W. R. III , Properties of the spindle-to-cusp transition in extensional capsule dynamics, *Europhys. Lett.* **106**, 48003 (2014).

[22] P. Dimitrakopoulos, Effects of membrane hardness and scaling analysis for capsules in planar extensional flows, *J. Fluid Mech.* **745**, 487-508 (2014).

[23] W.R. Dodson III and P. Dimitrakopoulos, Tank-treading of swollen erythrocytes in shear flows, *Phys. Rev. E* **85**, 021922(2012)

[24] W.R. Dodson III and P. Dimitrakopoulos, Oscillatory tank-treading motion of erythrocytes in shear flows, *Phys. Rev. E*,**84**, 011913 (2011)

[25] P. Dimitrakopoulos and Park Sun-Young, Transient dynamics of an elastic capsule in a microfluidic constriction, *Soft Matter* **9**, 8844-8855 (2013).

[26] Dimitrakopoulos and S. Kuriakose, Deformation of an elastic capsule in a rectangular microfluidic channel, *Soft Matter* **9**, 4284-4296 (2013).

[27] Y. Wang and P. Dimitrakopoulos, Low-Reynolds-number droplet motion in a square microfluidic channel, *Theor.Comput. Fluid Dyn.* **26**, 361-379 (2012).

[28] P.Dimitrakopoulos and S. Kuriakose, Motion of an elastic capsule in a square microfluidic channel, *Phys. Rev. E* **84**, 011906 (2011).

[29] S.K. Doddi and P. Bagchi, Lateral migration of a capsule in a plane Poiseuille flow in a channel, *Intl J. Multiphase Flow* **34**, 966-986 (2008).

[30] W. R. Dodson III and P. Dimitrakopoulos, Dynamics of strain-hardening and strain-softening capsules in strong planar extensional flows via an interfacial spectral boundary element algorithm for elastic membranes, *J. Fluid Mech.* **641**, 263-296 (2009).

[31] W. R. Dodson III and P. Dimitrakopoulos, Spindles, cusps and bifurcation for capsules in Stokes's flow, *Phys. Rev. Lett.* **101**, 208102 (2008).

[32] P. Dimitrakopoulos, Interfacial dynamics in Stokes flow via a three-dimensional fully-implicit interfacial spectral boundary element algorithm, *J. Comp. Phys.* **225**, 408-426 (2007).

[33] Yechun Wang and P. Dimitrakopoulos, Three-dimensional spectral boundary element algorithm for interfacial dynamics in Stokes flow, *Phys. Fluids* **18**, 082106(1-16) (2006).

[34] T. M. Geislinger, and T. Franke, Sorting of circulating tumor cells (MV3-melanoma) and red blood cells using non-inertial lift, *Biomicrofluidics* **7**, 044120 (2013)

[35] T. M. Geislinger, B. Eggart, S. Braunmuller, L. Schmid, and T. Franke, Separation of blood cells using hydrodynamic lift, *Appl. Phys. Lett.* **100**, 183701 (2012).

[36] H.L. Goldsmith, Red cell motions and wall interactions in tube flow, *Fed. Proc.* **30**, 1578–1590 (1971).

[37] R. Langer, Drug delivery and targeting, *Nature* **392** 5-10 (1998).

[38] W. Lee, P. Tseng, and D. Di Carlo, *Microtechnology for Cell Manipulation and Sorting*, Springer International Publishing (2017).

[39] V. A. Lubarda, *Elastoplasticity theory.* CRC Press, Boca Raton (2002).

[40] A.X. Lu, K. Jiang, D.L. DeVoe, and S.R. Raghavan, Microfluidic Assembly of Janus-Like Dimer Capsules, *Langmuir* **29** 13624-13629 (2013)

[41] A. Madene, M. Jacquot, J. Scher, and S. Desobry, Flavour encapsulation and controlled release - a review, *Int. J. Food Sci Technol* **41**, 1-21 (2006).

[42] N. Mohandas and J. A. Chasis, Red blood cell deformability, membrane material properties and shape: regulation by transmembrane, skeletal and cytosolic proteins and lipids, *Semin. Hematol.* **30**, 171-192 (1993).

[43] G. P. Muldowney and J. J. L. Higdon, A spectral boundary element approach to three-dimensional Stokes flow, *J. Fluid Mech.* **298**, 167 -192 (1995).

[44] Martin P. Neubauer, Melanie Poehlmann, and Andreas Fery, Microcapsule mechanics: From stability to function, *Advances in Colloid and Interface Science* **207** 65-80 (2014)

[45] Pavel Neuzil, Stefan Giselbrecht, Kerstin änge, Tony Jun Huan and Andreas Manz, Revisiting lab-on-a-chip technology for drug discovery, *Nature Reviews Drug Discovery* **11**, 620 - 632 (2012)

[46] Hiroshi Noguchi and Gerhard Gompper, Shape transitions of fluid vesicles and red blood cells in capillary flows, *PNAS* **102**, 14159-14164 (2005).

[47] C. Pozrikidis, *Computational Hydrodynamics of Capsules and Biological Cells.* Chapman and Hall/CRC (2010)

[48] C. Pozrikidis, *Modeling and Simulation of Capsules and Biological Cells.* Chapman and Hall/CRC (2003)

[49] F. Risso, F. Collé-Paillot, and M. Zagzoule Experimental investigation of a bioartificial capsule flowing in a narrow tube, *J. Fluid Mech.* **547**, 149-173 (2006).

[50] Ping-Wei Ren, Xiao-Jie Ju, Rui Xie, Liang-Yin Chu, Monodisperse alginate microcapsules with oil core generated from a microfluidic device, *J.Colloid and Interface Science* **343**, 392-395 (2010).

[51] Varna Sharma, Michael Hunckler, Melur K. Ramasubramanian, Emmanuel C. Opara, and Kalyan Katuri, Microfluidic Approach to Cell Microencapsulation, *Cell Microencapsulation: Methods and Protocols* **1479**,71 - 76 (2017)

[52] R. Skalak, A. Tozeren, R. P. Zarda and S. Chien, Strain energy function of red blood cell membranes, *Biophys. J.* **13**, 245-264 (1973).

[53] J. M. Skotheim and T. W. Secomb, Red blood cells and other nonspherical capsules in shear's flow: oscillatory dynamics and the tank-treading-to-tumbling transition, *Phys. Rev.Lett.* **98**, 078301 (2007).

[54] M. Sugihara-Seki, T. W. Secomb, and R. Skalak, Two-dimensional analysis of two-file flow of red cells along capillaries, *Microvascular Research* **40** 379 - 393 (1990).

[55] T. W. Secomb, R. Skalak, N. Özkaya, and J. F. Gross, Flow of axisymmetric red blood cells in narrow capillaries, *J. Fluid Mech.* **163**, 405 - 423 (1986).

[56] Yechun Wang and P. Dimitrakopoulos, Nature of the hemodynamic forces exerted on vascular endothelial cells or leukocytes adhering to the surface of blood vessels, *Phys. Fluids* **18**, 087107(2006).

[57] B.B.C. Youan , T.L. Jackson, L. Dickens , C. Hernandez C, G. Owusu-Ababio, Protein release profiles and morphology of biodegradable microcapsules containing an oily core, *J Control Release* **76**, 313-26 (2001).

Vita

Pompon Mputu Udipabu was born in May 1989, in the Democratic Republic of Congo. He was admitted to the University of Maryland at College Park in September 2007. In May 2012, he graduated and received a Bachelor of Science degree in Biochemistry and a Bachelor of Science degree in Chemical and Biomolecular Engineering. After graduation, Pompon started working at MedImmune, in Frederick, Maryland. He was involved in technology transfer and process characterization of an immunotherapy cancer drug, Keytruda. He remained at MedImmune until Keytruda was approved in 2014. While at MedImmune, Pompon enrolled in the Chemical and Biomolecular Engineering Graduate Program at the University of Maryland, College Park, in September 2013. In February 2014, under the guidance of Professor Panagiotis Dimitrakopoulos, he started conducting research regarding the dynamics of elastic capsules in T-jucntion and cross-junction mirofluidic channels. In April 2015, he started working as Process Engineer at Merck, in Elkton, Virginia. His duties involve process optimization and manufacturing operations of Lantus biosimalar, Lusduna. In May 2017, he is defending his dissertation for the Master of Science degree, entitled "Dynamics of an elastic capsule in cross-junction and T-junction microfluidic channels".

Publications and Presentations

Publication

- P. M. Udipabu and P. Dimitrakopopoulos, "Dynamics of an elastic capsule in a microfluidic cross-junction". *To be submitted* (2017).
- P. M. Udipabu and P. Dimitrakopopoulos, "Motion of an elastic capsule in a microfluidic T-junction". *To be submitted* (2017).

Presentations

- P. M. Udipabu and P. Dimitrakopopoulos, "Capsule dynamics in a microfluidic cross-junction", 13th Annual Symposium of the Burgers Program for Fluid Dynamics, University of Maryland, College Park, November 2016.
- P. M. Udipabu and P. Dimitrakopopoulos, "Capsule motion in a microfluidic cross-junction", 87th Annual Meeting of The Society of Rheology, Baltimore, Maryland, October 2015.
- P. M. Udipabu and P. Dimitrakopopoulos, "Capsule dynamics in a microfluidic T-junction", 11th Annual Symposium of the Burgers Program for Fluid Dynamics, University of Maryland, College Park, November 2014.